JBC Papers in Press. Published on February 24, 2015 as Manuscript M115.636894
The latest version is at http://www.jbc.org/cgi/doi/10.1074/jbc.M115.636894

HISTONE H2A AND H4 N-TERMINAL TAILS ARE POSITIONED BY THE MEP50 WD-REPEAT PROTEIN FOR EFFICIENT METHYLATION BY THE PRMT5 ARGININE METHYLTRANSFERASE

Emmanuel S. Burgos[1,4], Carola Wilczek[1,3,4], Takashi Onikubo[1], Jeffrey B. Bonanno[1], Janina Jansong[2], Ulf Reimer[2] and David Shechter[1,*]

[1]*Department of Biochemistry, Albert Einstein College of Medicine of Yeshiva University, Bronx, NY 10461;* [2] *JPT Peptide Technologies GmbH, Volmerstrasse 5, 12489 Berlin, Germany*
[4]*Contributed equally*
[3]*Current address: Erdmann Technologies GmbH, Fabeckstraße 60-62 14195 Berlin, Germany*
**For correspondence: David Shechter; david.shechter@einstein.yu.edu*

CAPSULE

Background: PRMT5-MEP50 is an arginine methyltransferase with significant roles in development and cancer.

Results: MEP50 binds to the histone fold domain and is essential for PRMT5's efficient use of SAM.

Conclusion: MEP50 is essential for methylation of histones H4 and H2A by PRMT5.

Significance: The mechanism of histone methylation by PRMT5-MEP50 provides novel insight for methyltransferase mechanisms and therapeutic development.

ABSTRACT

The protein arginine methyltransferase PRMT5 is complexed with the WD-repeat protein MEP50 (also known as Wdr77 or androgen coactivator p44) in vertebrates in a tetramer of heterodimers. MEP50 is hypothesized to be required for protein substrate recruitment to the catalytic domain of PRMT5. Here we demonstrate that the cross-dimer MEP50 is paired with its cognate PRMT5 molecule to promote histone methylation. We employed qualitative methylation assays and a novel ultrasensitive continuous assay to measure enzyme kinetics. We demonstrate that neither full-length human PRMT5 nor the *Xenopus laevis* PRMT5 catalytic domain have appreciable protein methyltransferase activity. We show that histones H4 and H3 bind PRMT5-MEP50 more efficiently compared to histone H2A(1-20) and H4(1-20) peptides. Histone binding is mediated through histone fold interactions as determined by competition experiments and by high density histone peptide array interaction studies. Nucleosomes are not a substrate for PRMT5-MEP50, consistent with the primary mode of interaction via the histone fold of H3/H4, obscured by DNA in the nucleosome. Mutation of a conserved arginine (R42) on the MEP50 insertion loop impaired the PRMT5-MEP50 enzymatic efficiency by increasing its histone substrate K_m, comparable to that of *Caenorhabditis elegans* PRMT5. We show that PRMT5-MEP50 prefers unmethylated substrates, consistent with a distributive model for dimethylation and suggesting discrete biological roles for mono- and dimethylarginine modified proteins. We propose a model in which MEP50 and PRMT5 simultaneously engage the protein substrate, orienting its targeted arginine to the catalytic site.

INTRODUCTION

Protein arginine methyltransferases (PRMTs) methylate arginines in histones and other proteins (1). Type I enzymes mono- and

asymmetrically-dimethylate arginine (Rme1 and Rme2a) (2). PRMT5 is a Type II enzyme that catalyzes arginine mono- and symmetric-dimethylation (Rme1 and Rme2s). PRMT5's many targets include ribosomal proteins, the histone chaperone Nucleoplasmin, p53, and histones (2-7). We and others showed that PRMT5 require the WD-repeat protein MEP50 (Methylosome Protein 50, also known as Wdr77 or androgen coreceptor p44) in vertebrates (8-12), while it is active independent of MEP50 in *Caenorhabditis elegans*. PRMT5 also partners with other co-factors (10,12-18). PRMT5-MEP50's expression and activity are now clinically correlated with poor prognosis in a range of cancers, suggesting that insight into its enzymatic mechanism will be essential for highly targeted drug design potential leading to new therapeutics (19-21).

Since PRMT5 methylates multiple histone and non-histone arginines *in vivo*, a long-standing question is how PRMT5 selects among these many sites and multiple protein targets. Our previous work using crystallography, qualitative binding studies, and electron microscopy reconstruction suggested that substrate recruitment was primarily mediated by the MEP50 subunit. The structure of *Xenopus laevis* PRMT5-MEP50 that we solved (22) and the human PRMT5-MEP50 structure solved by Emtage and colleagues (23) revealed a buried and poorly accessible catalytic site. These observations are consistent with a conserved and significant stringency in substrate selection.

MEP50 is a seven-bladed WD-repeat protein that is unusually acidic. We previously hypothesized that MEP50 served as a substrate presenter, similar to the initial hypothesis for the WD-repeat protein Wdr5 (24) and RbAp48 (25) in binding histones H3 and H4, respectively. Our crystal structure of the *Xl*PRMT5-MEP50●SAH complex and our electron microscopy reconstruction of the complex bound to its substrate Nucleoplasmin supported this hypothesis. We and others previously showed that human PRMT5 is inactive in the absence of MEP50, consistent with a required role in binding substrate.

Quantitative enzymatic analysis of methyltransferases requires ultrasensitive techniques due to their low turnover. Previously described kinetic assays are either not commercially available, have low throughput, or provide signals too low to be of use for slow enzymes such as PRMT5. Therefore, we employ a novel ultrasensitive coupled continuous assay to measure kinetic parameters of other methyltransferases previously introduced by our colleagues (26).

Here, we test the function of MEP50 in promoting PRMT5 histone methyltransferase activity. We employ structural analysis as well as qualitative and quantitative methylation assays to measure enzymatic activity and binding affinity for histones to PRMT5-MEP50. We show that mutation within the MEP50 insertion finger impaired kinetic parameters of both histone and SAM substrates. Our results support the concept that MEP50 interacts directly with histones and the N-terminal domain of PRMT5 but may also contribute to active site remodeling in PRMT5's C-terminal domain for efficient methyltransfer. Our computational modeling revealed multiple modes of substrate-enzyme interaction consistent with our experimental data. These studies support the essential function of MEP50 in binding histone fold and presenting histone tail substrate to the active site of PRMT5 cross-dimer for efficient methylation.

EXPERIMENTAL PROCEDURES

Reagents— Chemicals and reagents were obtained from Sigma, Fisher Scientific, or Research Products International. [^{3}H]-methyl- and [^{14}C]-methyl-SAM were purchased from Perkin-Elmer. SAM and SAH were purified by HPLC (Luna C18(2), Phenomenex), desalted, concentrated, and stored at −80°C (26). Reducing agent Tris(hydroxypropyl)-phosphine (THP) was from Novagen. ATP detection was achieved using ATPLite 1Step (Perkin-Elmer); molecular biology grade water, with additional charcoal treatment, was used for all enzymatic assays. DNase I was from New England Biolabs.

Proteins and peptides— *Xenopus laevis* PRMT5-MEP50 complex was produced and purified as described (5). *Xl*MEP50 mutagenesis was performed by mutating R42 (codon: CGC) to glutamine (Q, codon: CAG) or glutamic acid (E, codon: GAG). Corresponding baculoviruses were produced in DH10Bac cells (Invitrogen), followed by co-infection of Hi5 cells with wild-type *Xl*PRMT5. Cell lysis, Nickel-affinity chromatography, Superdex 200 gel filtration and concentration were performed as before (22). Wild-type *Xl*MEP50 and mutants (R42Q, R42E) were obtained in excess when purifying corresponding *Xl*PRMT5-MEP50 complexes. Recombinant *Xenopus laevis* core histones were expressed as 6xHis-Tag TEV (H2A, H3, H4) fusions proteins and the tag was completely removed by TEV protease to leave a scarless histone. Recombinant Nucleoplasmin from *Xenopus laevis* was expressed and purified as previously described (22). The H4(1-7) and H4(1-20) peptides were from AnaSpec Inc. (Cat # 62754 and 62498, respectively); all other peptides were prepared by the peptide synthesis facility at the Rockefeller University. Recombinant Flag-*Hs*PRMT5 enzyme was purchased from SinoBiologicals (Cat # 11074-H18H; Beijing, China). Recombinant *Xenopus* mononucleosomes were purchased from Epicypher (Cat # 16-0005) and octamers were produced as described (22). Enzymes for luciferase-based assay, including the *Clostridium symbiosum* pyruvate phosphate dikinase (*Cs*PPDK; generous gift provided by Dr. Debra Dunaway-Mariano, University of New Mexico), the adenosine phosphoribosyltransferase from *Saccharomyces cerevisiae* and the 5'-methylthioadenosine/*S*-adenosyl-L-homocysteine nucleosidase from *Salmonella enterica* (*Sc*APRT and *Se*MTAN, respectively; generous gift from Dr. Vern L. Schramm, Albert Einstein College of Medicine), were expressed and purified to homogeneity according to published protocols (27,28).

Filter binding methyltransferase assay and fluorography— Assays were performed as described (22). Briefly, substrate protein was incubated with PRMT5-MEP50 enzyme at the indicated concentrations in 15 µl reaction buffer (20 mM Tris pH 8.0, 10 mM DTT, protease inhibitors, 0.5 µM [^{3}H]-methyl-SAM of specific activity 78.2 Ci mmol^{-1}) for 20 min at 30°C. The reaction mixture was spotted on P81 filter paper, washed with sodium carbonate buffer (0.1 M, pH 8.5), air-dried and analyzed via scintillation counter (Wallac Winspectral 1414 LSC). Alternatively, the reaction mixture was run on an SDS-PAGE gel, stained and imaged, soaked in Amplify (NAMP100, GE), dried and exposed to film.

Nucleosome methyltransferase assay— Assay was performed with 2 µg of mononucleosomes treated with 2 units of DNase I or reaction buffer alone for 1.5 hours at 30 ºC prior to addition of *Xl*PRMT5-MEP50 (300 nM final concentration) in presence of [^{3}H]-methyl-SAM (0.3 µM final concentration; specific activity 78.2 Ci mmol^{-1}). Similar experiments using recombinant H2A and H4 (2.5 µM) were run in parallel. After 20 min, reaction mixtures were run on an SDS-PAGE gel, stained and imaged, soaked in Amplify (NAMP100, GE), dried and exposed to film.

Flag-pulldown— Anti-Flag M2 antibody-coupled agarose beads (20 µL) were incubated with equimolar amounts (50 nM) of *Xl*MEP50 (wild-type or mutants) and Flag-tagged *Hs*PRMT5 in 250 µl TBS (150 mM NaCl, Tris-HCl pH 8.0) at 4°C for 2 hours. As a negative control, *Xl*MEP50 was incubated under the same conditions without *Hs*PRMT5. The suspension was then transferred to a Mini-spin column (USA scientific) and centrifuged (30 s, 500 × *g*). After intense washing with TBS, the beads were boiled for 10 min in SDS loading dye for elution. The elution samples were analyzed via SDS-PAGE and western blot with α-PRMT5 (Millipore) and α-MEP50 antibodies.

Luciferase-based coupled assay buffer— The formation of SAH as a product of the methyltransferase reaction was monitored using a previous reference with the following coupling enzymes *Cs*PPDK (4.6 mU/well), *Sc*APRT (250 µU/well) and *Se*MTAN (14 µU/well) (26). The 20× concentrated buffer B1 (1.0 M Tris-acetate pH 7.7, 20 mM PEP, 20 mM PPi, 150 mM ammonium sulfate and 20 mM PRPP; treated with charcoal and filter sterilized) was supplemented with $MgCl_2$ (10 mM), THP (1 mM), ATPlite 1Step (*note:* the Perkin-Elmer substrate buffer solution supplied in this kit inhibits *Xl*PRMT5-MEP50 and was replaced by a 50 mM Tris-acetate buffer), *Cs*PPDK, *Sc*APRT and *Se*MTAN. Then the histones/peptide substrates and *Xl*PRMT5-MEP50 enzyme complex or *Ce*PRMT5 were added to prepare the final buffer B2. Each experiment used 40 µL of B2.

Luciferase-based coupled enzymatic assays— Kinetic parameters were determined at 25°C by monitoring luminescence using a SpectraMax L instrument configured with two photomultipliers (photo counting mode; Molecular Devices) in a 96-well half-area flat bottom plate (Corning; Cat # 3992). Luminescence is measured in relative light units (RLU). Briefly, 40 µL of buffer B2 (containing 20-200 nM PRMT5 enzymes) was mixed with SAM substrate (10 µL of 125 µM solution, final saturating concentration of SAM at 25 µM; higher saturating concentrations are required for mutants with higher SAM K_m). Under our experimental conditions, the typical Michaelis–Menten model is not suited to characterize the behavior of PRMT5 from both *Xenopus laevis* and *Caenorhabditis elegans*. *In vitro*, these enzymes have poor activity with turnover rates k_{cat} as low as 20 h^{-1} and the use of high nanomolar concentration of methyltransferase is generally required. During the early stage of substrate titration (SAM or peptide substrates), enzyme and substrate concentrations have the same order of magnitude. Therefore a significant fraction of total substrate is bound to the enzyme (*i.e.* enzyme-substrate complex). The Morrison kinetic model accounts for this early substrate depletion (Equation 1). Therefore, initial rates were plotted against substrate concentrations and fitted to this kinetic model to yield corresponding K_m and k_{cat} values (29).

$$v = k_{cat}\,\frac{([E]_T+[S]_T+K_m)-\sqrt{([E]_T+[S]_T+K_m)^2-4[E]_T[S]_T}}{2} \quad (\textbf{\textit{Eq.}}\ \textbf{1})$$

where $[E]_T$ and $[S]_T$ are the total concentration of enzyme and substrate, respectively.

HPLC separation of histones— Histones H4 (RT = 26.5 min), H2A (RT = 28.9 min), *TL*H2A (RT = 32.0 min) and H3 (RT = 42.5 min) were separated onto a reverse phase C_8 column (Vydac; Cat# 228TP101, 300Å, 10 µm, 1.0 x 250 mm) at 65°C using mobile phases A (water, 0.1% TFA) and B (acetonitrile, 0.1% TFA) according to the following gradient: 0-3.57 min (SAM, small peptides and salts removal; 95% A), 3.57-21 min (linear to 65% A), 21-46 min (histones' separation; linear to 62% A), 46-47 min (linear 10% A), 47-57 (higher MW proteins' removal;

constant 10% A), 57-58 min (linear 95% A), 58-78 min (equilibration; constant 95% A).

*Competition experiments between histone H2A and other histones/peptides for binding onto Xl*PRMT5-MEP50 or *Ce*PRMT5— Experiments were performed in 100 μL total volume with 50 mM MOPS pH 7.0, 100 nM *Xl*PRMT5-MEP50 or 100 nM *Ce*PRMT5, 20 μU *Se*MTAN, histone H2A with concentration kept at 2.0 μM, increasing amounts of histone/peptide substrates (0-12.6 μM final concentration) and 1 mM THP. Reactions were initiated by adding 80 μL of the above samples to PCR tubes already loaded with 20 μL of SAM reagent (25 μM final [^{3}H]-methyl-SAM concentration; 10 μCi per reaction). After 15 min at 25°C, TFA (3 μL, 10% v/v) was added to quench the reactions. Samples are kept at -80°C before processing by HPLC. Methyltransfer onto histone H2A was then quantified by liquid scintillation counting and plotted against matching concentrations of histone/peptide competitors.

*Binding affinity of histone H2A for Xl*MEP50 *and Xl*PRMT5-MEP50— *Xl*MEP50 was freshly prepared; a gel filtration was used as the last purification step (25 mM ADA, 100 mM NaCl, 1 mM βME, pH 6.5). Samples were prepared as described for the luciferase-based assay, with *Xl*PRMT5-MEP50 and histone H2A concentration set at 100 nM and 2.0 μM, respectively. Exogenous *Xl*MEP50 was added (0-20 μM) and samples' composition was kept constant (adjusted with gel filtration buffer: 25 mM ADA, 100 mM NaCl, 1 mM βME, pH 6.5). Methyltransfer started upon addition of SAM (25 μM final concentration). During the event, exogenous MEP50 (*M*) and PRMT5-MEP50 (*P/M*) compete for H2A (*H*) binding where the histone fold can bind to MEP50, forming the $M^*\bullet H$ and $P/M^*\bullet H$ complexes, respectively. Methyltransfer occurs when the complex $P^*/M^*\bullet H$ is formed (the histone fold is bound to the MEP50 presenter and the histone tail is bound to the enzyme active site). The following relationships can be written:

$[H]_T = [H]_{free} + [P/M^*\bullet H] + [P^*/M^*\bullet H] + [M^*\bullet H]$, the total histone concentration simplified as $[H]_T = [H]_{free} + [M^*\bullet H]$, since $[H]_T >> [P/M]_T$ (*i.e.* 2.0 μM >> 100 nM). Likewise, $[M]_T = [M]_{free} + [M^*\bullet H] + \beta[M]_T$, the total MEP50 concentration with the factor β accounting for potential aggregation/misfolding of MEP50 occurring along the titration experiments (a value between 0 and 1, with $\beta = 0$ corresponding to no aggregation/misfolding of MEP50).

Considering the binding between exogenous MEP50 and full-length histone, the following expressions can be written,

$$K_d' = \frac{[H]_{free}[M]_{free}}{[M^*\bullet H]} = \frac{k_{-3}}{k_3} = \frac{[H]_{free}([M]_T - [M^*\bullet H] - \beta[M]_T)}{[H]_T - [H]_{free}} = \frac{[H]_{free}(1-\beta)[M]_T - [H]_{free}[H]_T + [H]_{free}^2}{[H]_T - [H]_{free}} \quad (\textbf{\textit{Eq. 2}})$$

also equivalent to $[H]_{free}^2 + ((1\text{-}\beta)[M]_T - [H]_T + K_d')[H]_{free} - K_d'[H]_T = 0$ and solved for the $[H]_{free}$ concentration:

$$[H]_{free} = \frac{1}{2}(-((1-\beta)[M]_T - [H]_T + K_d') + \sqrt{((1-\beta)[M]_T - [H]_T + K_d')^2 + 4K_d'[H]_T}) \quad (\textbf{\textit{Eq. 3}})$$

Considering the methyltransfer reaction, the following relationships can be written,

$$K_d = \frac{[P/M][H]_{free}}{[P/M^*\bullet H]} = \frac{k_{-1}}{k_1} \quad \text{and by analogy,} \quad K_m = \frac{k_{-2}}{k_2} = \frac{[P/M^*\bullet H]}{[P^*/M^*\bullet H]}$$

$$\frac{V}{[E]_T} = \frac{k_{cat}[P^*/M^*\bullet H]}{[P/M] + [P/M^*\bullet H] + [P^*/M^*\bullet H]} \quad (\textbf{\textit{Eq. 4}})$$

The equation 4 is rearranged using K_m and K_d relationships leading to the expression of v/V_{max}:

$$\frac{v}{V_{max}} = \frac{\frac{1}{K_d K_m}[P/M][H]_{free}}{[P/M]+\frac{1}{K_d}[P/M][H]_{free}+\frac{1}{K_d K_m}[P/M][H]_{free}} = \frac{[H]_{free}}{K_d K_m\left(1+\frac{[H]_{free}}{K_d}\right)+[H]_{free}} \quad (\textbf{\textit{Eq. 5}})$$

Finally, the solution for $[H]_{free}$ (Equation 3) is replaced in the v/V_{max} velocity expression to obtained both K_d and K_d'. Ratios between experimental initial (v) and maximal (V_{max}) velocities were plotted against exogenous *Xl*MEP50 concentrations and fitted to our binding model (Equation 5) where $[M]_T$ and $[H]_T$ are the total concentrations of MEP50 and histone H2A, respectively, $[H]_{free}$ is the free concentration of histone H2A at equilibrium, K_m is the Michaelis constant for histone H2A when used as a substrate with *Xl*PRMT5-MEP50, K_d' is the dissociation constant of histone H2A from the complex *Xl*MEP50●H2A, K_d is the dissociation constant of histone H2A from *Xl*MEP50 already complexed with *Xl*PRMT5 (*Xl*PRMT5-MEP50●H2A).

Peptide array binding studies─ A library of 20-mer peptides spanning the sequences of histones was generated with or without known modifications and in various combinations (sequences available at www.jpt.com), as previously described (22). For binding studies, Flag-*Hs*PRMT5 and *Xl*MEP50 were pre-incubated in equimolar amounts (66.5 nM) in KCl/HEPES buffer for 30 min at room temperature to form a complex. The complex was applied to individual histone code peptide microarrays for one hour at 30°C. For detection of binding events the microarrays were incubated with anti-FLAG mouse monoclonal antibody (Pierce, #MA1-91878) or anti-MEP50 rabbit polyclonal antibody. Upon washing and incubation with fluorescently labeled antibody (DyLight649-anti-mouse IgG; Thermo #35515 or DL649-anti-rabbit IgG; Pierce, #35565) the microarrays were washed again and dried. Incubation with primary and secondary antibody alone was used as a control. Each microarray was scanned using GenePix Autoloader 4200AL (Molecular Devices, Pixel size: 10 µm). Signal intensity was evaluated using GenepixPro software (Molecular Devices). Further evaluation and representation of results was performed using the R statistical programming system (Version 2.11.1, www.r-project.org).

Structural alignments, binding site predictions, and rigid body docking─ All structural figures were visualized using VMD v1.9.1 (30). Structural alignments were performed using the STAMP and Multiseq alignment tools within VMD (31,32). Rigid body docking was performed at the ClusPro 2.0 server (http://cluspro.bu.edu) (33,34).

ClusPro 2.0 docking- Docking of H2A/H2B and H3/H4 histone dimers was done using the following attractive residues. Residue numbers (listed as PDB chain letter – residue #) in PRMT5, MEP50, and histones used for attraction in rigid-body docking in ClusPro 2.0. Chain Y is the cross-dimer MEP50 from Chain Q PRMT5. Chain C and D are H2A and H2B with the N-terminal tails removed, chain A and B are H3 and H4 with the N-terminal tails removed. The residues below were assigned attractive forces in ClusPro.

For H2A/H2B dimer docking─ Receptor attraction: Y-16 Y-19 Y-20 Y-38 Y-39 Y-40 Y-41 Y-42 Y-43 Y-44 Y-45 Y-68 Y-70 Q-318 Q-324 Q-366 Q-386 Q-396 Q-400 Q-404; ligand attraction: C-21 C-22 C-23 C-24 C-25 C-26 C-27 C-28 C-29 C-30 C-31 C-32 C-33 C-34 C-35 C-36 C-37 D-31 D-32 D-33 D-34 D-35 D-36 D-37.

For H3/H4 dimer docking─ Receptor attraction: Y-16 Y-19 Y-20 Y-38 Y-39 Y-40 Y-41 Y-42 Y-43 Y-44 Y-45 Y-68 Y-70 Q-318 Q-324 Q-366 Q-386 Q-396 Q-400 Q-404; ligand attraction: A-61 A-62 A-63 A-64 A-65

A-66 A-67 A-68 A-69 A-70 B-24 B-25 B-26 B-27 B-28 B-29 B-30 B-31 B-32 B-33 B-34 B-35 B-36 B-37 B-38 B-39 B-40 B-85 B-86 B-87 B-88 B-89 B-90 B-91 B-92 B-93 B-94 B-95 B-96 B-97 B-98 B-99 B-100 B-101 B-102 B-103 B-104.

RESULTS

Our previous work defined two distinct relative classes of MEP50 molecules within the PRMT5-MEP50 tetramer: the directly-bound MEP50 and the cross-dimer MEP50 (22). Additionally, both our solved *Xenopus laevis* PRMT5-MEP50 structure and the solved human complex structure (23) demonstrated unique N- and C-terminal domains of PRMT5 simply connected by a loop. Based on its structural organization, residue conservation, and our electron microscopy images of *Xl*PRMT5-MEP50 complexed with substrate, we hypothesized that the cross-dimer MEP50 is responsible for organizing substrate for the PRMT5 catalytic domain.

Structural arrangement of PRMT5 and MEP50— To test the conserved structural relationships between MEP50 and the distinct N- and C-terminal domains of PRMT5, we performed Cα-carbon backbone alignments between the *Xenopus laevis* and human PRMT5-MEP50 structures (PDB:4G56 and 4GQB, respectively) (Figure 1A) using the STAMP alignment tool in VMD MultiSeq (31,32). First we aligned only the entire PRMT5 molecule (as indicated by the black box in 1B and schematic in 1A) and plotted the per-residue Cα RMSD values (Å) for PRMT5 (purple) and both MEP50 molecules (directly bound = pink and cross-dimer = blue) (Figure 1B, top row). PRMT5 itself was only modestly well aligned, with many regions containing an RMSD >2 Å. The directly-bound MEP50 was induced into modest alignment by PRMT5, while the cross-dimer MEP50 was not aligned well at all. When we aligned the PRMT5 N-terminal domain that directly contacts MEP50, we observed tight alignment (RMSD <2 Å) for the PRMT5 domain as well as the directly bound MEP50 (Figure 1B, second row).

When we aligned the C-terminal domain of PRMT5 that does not directly contact either MEP50, we observed no alignment of the directly bound MEP50 but strong alignment of the cross-dimer MEP50 (RMSD <2 Å, Figure 1B, third row). Despite the different crystal forms of the solved structures which could possibly lead to packing artifacts, this relationship is strikingly apparent. Therefore, we concluded that a conserved relationship between the catalytic C-terminal domain of PRMT5 and the cross-dimer, but non-contacting MEP50 exists. This relationship is unlikely to be allosteric due to the multiple domain boundaries and inter-molecule contacts that would be required to communicate this information.

XlPRMT5 catalytic domain is inactive— We and others previously demonstrated that PRMT5 alone has exceedingly modest histone methyltransferase activity in the absence of MEP50 (22,23). Since we showed in Figure 1 that a functional relationship likely exists between the catalytic domain of PRMT5 and the cross-dimer MEP50, we produced recombinant *Xl*PRMT5 catalytic domain (PRMT5ΔN, residues 291-633) to test if the catalytic domain alone was active. This truncated protein was soluble in *E. coli* and sedimented primarily as monomer in analytical ultracentrifugation (Figure 2A; *not shown*). We then measured *Xl*PRMT5(291-633) enzymatic activity using the filter-binding methyltransferase assay on multiple known peptide and protein substrates of PRMT5-MEP50, in the absence or presence of MEP50 (Figure 2B). *Xl*PRMT5(291-633) did not exhibit any activity on any of these substrates, while intact full-length *Hs*PRMT5 did recover activity with *Xl*MEP50 added *in trans*. A one-year exposure of a fluorogram did reveal very low levels of histone methyltransferase activity by full-length *Hs*PRMT5 in the absence of *Xl*MEP50, compared with robust activity of the *Xl*PRMT5-MEP50 complex or *Xl*MEP50 added *in trans* to

*Hs*PRMT5 (Figure 2C). We concluded from these experiments that only the full-length PRMT5-MEP50 complex is able to efficiently methylate its substrates.

To demonstrate the strict requirement for MEP50 in promoting PRMT5 histone methyltransferase activity, we titrated *Xl*MEP50 with constant *Hs*PRMT5 and measured histone H2A methylation in the filter binding assay. We observed a MEP50 dose-dependent increase in activity maximal at the 4:4 stoichiometry with PRMT5, consistent with a required role for MEP50 in organizing substrate (Figure 2D).

Histone affinities for XlPRMT5-MEP50— Our results to this point implicate MEP50 in its essential function in promoting PRMT5 methyltransferase activity. However, *in vivo,* PRMT5-MEP50 has distinct protein substrate selections in different contexts. In particular, H4R3 methylation is primarily observed on chromatin while H2A R3 methylation is observed on soluble, cytoplasmic histones (35-37). Soluble H2A is heterodimerized with H2B, but typically not complexed with H3/H4 in the cytoplasm or nucleus when in solution. Chromatin bound histones are all found within the same nucleosome embedded in DNA.

Therefore, to determine relative substrate preferences for PRMT5-MEP50, we performed methyltransferase assays with different combinations of histone proteins (H2A and H4, both methylated by PRMT5-MEP50) and assayed the activity by fluorography. First, we titrated full-length histone H4 into reactions with constant histone H2A (Figure 3A). Strikingly, methyltransfer onto histone H2A was readily inhibited by H4. To determine if this significant preference for H4 is due to direct competition of the histone tail containing R3, we performed a similar methyltransferase assay and titrated peptide H4(1-20) against histone H2A (Figure 3B). This peptide substrate was a poor competitor. Since all experiments were performed under initial velocity conditions, [^{14}C]-methyl-SAM depletion was not the cause of the loss of activity when using histone/peptide competitors. This observation suggested that the competition for *Xl*PRMT5-MEP50 may be primarily mediated through the histone-fold domain of H4.

The response observed with fluorography during film exposure is non-linear. To overcome the drawbacks of this technique, [^{3}H]-methyl transfer was quantified by liquid scintillation counting. We performed similar competition experiments and separated histones by reversed-phase HPLC (Figure 3C) (38). Our results confirmed the highly efficient histone H4 competition with histone H2A for R3 methylation (Figure 3D). Furthermore, histone tail peptide H4(1-20) inhibited methyltransfer toward H2A but to a lesser extend (*i.e.* 25% at 14 μM). With concentration levels 54X lower than the ones required when peptide H4(1-20) was used, the histone-fold domain of H4 appears to be critical for PRMT5-MEP50 complex binding and for competition with full length histone H2A.

PRMT5 dimethylates H3R8 *in vivo* (39-41) but *Hs*PRMT5-MEP50 poorly methylates H3 *in vitro* (42), so we tested the ability of histone H3 to displace the activity toward H2A (Figure 3D). PRMT5-MEP50 was unable to methylate histone H3 (no incorporation of ^{3}H-methyl at pH 7.0 when using 25 μM SAM and 100 nM enzyme). Yet we observed a strong competition between histones H3 and H2A. Although both histones H4 and H3 display similar competition for PRMT5-MEP50, the highest concentrations of H3 were insufficient to achieve complete inhibition of PRMT5 methylation of histone H2A. Our results suggest the presence of specific histone-fold binding regions for the *Xl*PRMT5-MEP50 complex.

CePRMT5 displays affinity for the histone-fold domain of H4 without assistance from a MEP50 binding partner— We tested the ability of *Ce*PRMT5 to bind the histone-fold domain using similar competition experiments with fixed concentration of H2A and increasing concentration of histone/peptide competitors. Although *Ce*PRMT5 does not associate with a MEP50 homologue, we did observe strong displacement of H2A by the H4 histone-fold domain in comparison to the H4(1-20) peptide (Figure 3E). Likewise, the non-substrate H3 competed efficiently against H2A for binding onto *Ce*PRMT5. These data suggest that both *Ce*PRMT5 and *Xl*PRMT5-MEP50 enzymes may have different binding mechanisms for their protein substrates.

Histone peptide array interaction studies— To further test our hypothesis that *Xl*PRMT5-MEP50 may bind histones H3 and H4 through their histone fold, which would explain the competition of H2A activity by these histones, we employed an extremely high density histone peptide array containing peptides covering the entire sequence of the core histones. We incubated Flag-*Hs*PRMT5 complexed with *Xl*MEP50 on the array and probed with anti-FLAG and anti-MEP50 antibodies. We extracted relative binding data from these assays and plotted the signal onto the core histone sequence (Figure 3F). Strikingly, the highest binding signals were obtained on histone fold or C-terminal peptides of histones H3 and H4. We also determined the influence of histone post-translational modifications on complex binding. In particular, pronounced loss of H4 C-terminal tail binding by *Hs*PRMT5/*Xl*MEP50 was observed upon phosphorylation of residue Y98 (*data not shown*). While this modification has not yet been observed *in vivo*, follow-up mass spectrometry and targeted bindings studies may specifically analyze this modification.

Furthermore, we quantified the binding affinity of histone H2A for both free *Xl*MEP50 and the *Xl*PRMT5-MEP50 complex, K_d' and K_d, respectively. We turned to a new ultrasensitive coupled enzymatic assay to monitor PRMT5-MEP50 activity upon addition of exogenous MEP50 under saturating concentration of SAM and fixe concentration of histone H2A (26). The assay couples conversion of SAM to SAH by PRMT5-MEP50 in a protein dependent fashion to downstream ATP and commensurate light production by luciferase. We expect addition of MEP50 to sequester H2A, thus preventing the histone from binding onto the PRMT5-MEP50 complex for further methylation (Figure 3G). As a result, light production would decreases with increasing concentration of exogenous MEP50 (Equations 3 and 5). We observed an affinity (K_d) of 1.78 ± 0.06 μM between H2A and PRMT5-MEP50 (Figure 3H), which is reminiscent of the K_m measured for H2A(1-20) and histone tails (Table 1). This result supports the observations from our peptide array study with H2A residues 1-30 being responsible for most of the binding onto PRMT5-MEP50 complex (Figure 3F).

Nucleosomes are not substrates for PRMT5-MEP50— We previously showed that PRMT5-MEP50 is incapable of methylation of nucleosomes *in vitro* (22). To conclusively test this inability to methylate the typical cellular state of histones, we incubated PRMT5-MEP50 with H2A, H4, and recombinant mononucleosomes in the absence or presence of DNase I with identical buffer conditions (Figure 4A). Mononucleosomes were not substrates of PRMT5-MEP50 compared to its significant methylation of free H2A and H4. After digestion of the DNA by DNase I, PRMT5-MEP50 did have H4 and H2A methyltransferase activity, confirming that DNA in the nucleosome directly inhibits the enzyme activity.

We used the results from our peptide array studies and mapped the domains of high binding for *Hs*PRMT5/*Xl*MEP50 onto the

nucleosome core structure. We found that these peptides contained residues on the lateral surface of H3/H4. Binding on this surface would likely position the targeted H4R3 towards the PRMT5 catalytic site (Figure 4B). Tight binding on this face would also orient the H2AR3 away from the catalytic site, consistent with the greater activity directed towards H4 in the competition assays above. Since the highest binding regions of the octamer for *Hs*PRMT5/*Xl*MEP50 lie on or adjacent to the DNA superhelical path on the nucleosome, these observations may explain the absence of methyltransferase activity towards nucleosomes.

Function of the MEP50 insertion finger— To test our hypothesis that MEP50 orients and presents substrate to the PRMT5 catalytic domain, we inspected the structures to determine potential residues to mutate. The *Xenopus laevis* and human PRMT5-MEP50 structures both contain a conserved MEP50 insertion finger that extends from the cross-dimer MEP50 and ends approximately 10 Å above the catalytic domain of PRMT5 (Figure 5A and boxed zoomed view). This insertion finger is directly on the surface that we initially hypothesized to be responsible for substrate presentation (22). *Xenopus laevis* MEP50R42 is 100% conserved among vertebrate MEP50 proteins (*i.e.* R52 in human MEP50), is at the terminus of the finger and is ~3.4 Å away from E403 of the cross-dimer PRMT5, potentially forming a salt-bridge to stabilize the finger (Figure 5A, boxed zoom view). We mutated this residue to glutamate or glutamine and produced PRMT5-MEP50$_{R42E}$ and PRMT5-MEP50$_{R42Q}$ protein complexes and MEP50$_{R42E}$ and MEP50$_{R42Q}$ alone (Figure 5B, 5C). The PRMT5-MEP50$_{R42E}$ and PRMT5-MEP50$_{R42Q}$ complexes were purified from insect cells in the same manner as the wild-type complex. MEP50$_{R42E}$ sedimented as a monomer in an analytical ultracentrifuge (*data not shown*). To confirm that MEP50 mutants interacted normally with PRMT5, we incubated the proteins with Flag-tagged *Hs*PRMT5 and both were enriched on anti-Flag resin just like wild-type MEP50 (Figure 5D).

To determine the ability or inability of MEP50 mutants to promote PRMT5 methyltransferase activity, we first used the filter binding assay. On multiple known peptide and protein substrates, MEP50$_{R42E}$ only promoted low levels of PRMT5 activity (Figure 5E). In contrast, the MEP50$_{R42Q}$ containing complex, without the charge reversal that would disrupt the putative salt-bridge, exhibited similar activity to the wild-type complex. These data support the hypothesis that cross-dimer interaction of MEP50 and the PRMT5 catalytic domain through MEP50 insertion loop is important for methyltransferase activity.

The filter binding assays are subject to some substantial error and do not report kinetic parameters in the end-point readout that we employed. Therefore, we used the luciferase-based coupled assay to determine K_m and k_{cat} of the *Xl*PRMT5-MEP50 and mutant complexes. Our kinetic parameters for PRMT5-MEP50, the MEP50$_{R42E}$ and MEP50$_{R42Q}$ complexes are shown in Figure 6A,B and in Table 1.

The PRMT5-MEP50$_{R42Q}$ and PRMT5-MEP50$_{R42E}$ complexes exhibit similar loss of catalytic efficiency with H4(1-20) peptide substrate when compared to wild-type PRMT5-MEP50 (Figure 6A; arrows with boxed change in efficiency values). Both mutations of residue R42 had similar impact on the turnover number k_{cat}, as mutants R42Q and R42E processed peptide substrate four times slower than the wild-type MEP50 (Figure 6C, top pink bar graph). However, unlike the R to Q mutation, the mutant R42E drastically impaired the binding of peptide substrate as its K_m was twenty-four times higher than the wild-type (Figure 6C,

top grey bar graph). These results are consistent with our hypothesis that the MEP50 insertion finger is critical for protein substrate binding.

To gain further insight into the possible interactions between MEP50 and its cross-dimer PRMT5, we determine the kinetic parameters for the SAM substrate using wild-type and MEP50R42 mutant complexes at saturating concentrations of H4(1-20) peptide substrate (Figure 6B). Surprisingly, the R to E mutation had the highest impact on the SAM K_m with values increasing from 3.3 to 27 μM when compared to the wild-type MEP50. The R to Q mutation only raised the K_m for the methyl donor by a factor of 1.6 (Figure 6C, bottom grey bar graph). To reduce potential interactions of peptide substrate with MEP50, we then measured kinetic parameters for SAM using the short peptide substrate H4(1-7) (Figure 6B). The PRMT5-MEP50$_{R42E}$ complex displayed a dramatic loss of affinity for SAM with a K_m 23-fold higher than that of wild-type complex (Table 1). The SAM substrate only binds to the PRMT5 active site. Therefore, our kinetic results suggest that MEP50 insertion loop is critical for histone binding and tail orientation and is also important for configuration of catalytically efficient PRMT5.

Kinetic parameters of XlPRMT5-MEP50 reveal substrate preferences— Our complete set of histone substrate kinetic parameters is shown in Table 1 and in Figure 6A and 6B as a semilog scatterplot of K_m vs k_{cat} (higher efficiency in the plot upper left, lower efficiency in lower right). The enzyme exhibited slow turnover with all substrates, on the order of 10-50 h^{-1}. The most efficient substrates were the (1-20) and (1-21) histone peptide tails from H4 and from H2A and H2A.X-F (also known as H2A.X.3), with catalytic efficiencies ranging from $2.9x10^4$ to $1.3x10^5$ M^{-1} s^{-1}. These kinetic parameters for peptide substrates are reminiscent of results reported by Thompson and co-workers using *Hs*PRMT5-MEP50 (42), though differences in N-terminal functionalization (amine vs acetyl) may account for subtle discrepancies (Table 1). Full-length histone H4 and Nucleoplasmin were also reasonably efficient substrates. The short H4 (1-7) peptide was a very poor substrate, consistent with our hypothesized role of MEP50 in organizing substrate.

Finally, we tested a monomethylated H2A.X-F R3me1 peptide in this assay to determine if PRMT5-MEP50 is likely to be processive or distributive in its catalysis of dimethylation. The R3me1 peptide was ~20-fold less efficiently methylated, with the majority of this effect embedded in the K_m, consistent with poor substrate binding. This result is reminiscent of the previously implicated distributive mechanism of catalysis to the dimethyl state (43,44). Additionally, we tested H2A and H4 mono- and dimethylation over time using specific antibodies. The accumulation of me2s depended on saturation of the me1 state in this assay. Although the use of antibodies is not quantitative, our results are likely incompatible with processive methylation model and suggest a distributive model (Figure 6D).

Prediction of histone binding sites onto XlPRMT5-MEP50 using computational docking— To determine potential interaction surfaces and residues on *Xl*PRMT5-MEP50, we used the SPPIDER (45) and PredUs (46) prediction algorithms and mapped the sites identified by both (Figure 7A). Then we docked tailless H2A-H2B dimers and H3-H4 tetramers (from PDB:1KX5) with *Xl*PRMT5-MEP50 in ClusPro 2.0 (33,34) using with experimental and predicted interaction constraints on PRMT5, MEP50, and the histones. These constraints included attractive forces on the histone regions identified on the peptide array binding studies and attractive forces on MEP50 R42 and the PRMT5-

MEP50 SPPIDER and PredUs predicted interaction sites. Sample output models for putative H2A-H2B and H3-H4 interactions are shown in Figure 8B and 8C, respectively. We conclude that our experimental and predicted binding domains are consistent with our MEP50 dependent model for histone substrate recognition.

DISCUSSION

Based on our published structure we previously proposed the "cross-dimer" model for MEP50 presentation of substrate to PRMT5. Here we used structural analysis, biochemistry, and enzymology to test our model of MEP50-dependent histone recognition and methylation by its coordinated PRMT5. These multiple approaches provided solid support for our hypothesis that MEP50 critically enhances the histone substrate methylation, and will help guide future studies to uncover specific mechanisms of recognition of other PRMT5 target proteins.

PRMT5-MEP50 structural and enzymatic conservation— The structural conservation of the arrangement of MEP50 in the complex with PRMT5 gave us initial support for our model due to the clear coordination of the cross-dimer MEP50 from the catalytic domain of PRMT5. We gleaned further understanding of the role of MEP50 through structural alignment of the *Xenopus laevis* PRMT5-MEP50 structure with the *Caenorhabditis elegans* PRMT5 in the absence of MEP50. We aligned the *Xl*PRMT5 N-terminal domain, contacting *Xl*MEP50, and the cross dimer *Xl*PRMT5 C-terminal catalytic domain, with the *Ce*PRMT5 chain and did not observe any regions of poor alignment, consistent with the absence of substantial allostery upon MEP50 binding.

Considering the relatively buried catalytic site in *Xl*PRMT5 and its tetrameric nature, it was formally possible that MEP50 was necessary to organize substrate to overcome the entropic cost for substrate binding to PRMT5. To test this possibility, we produced the catalytic C-terminal domain of *Xl*PRMT5 alone with the expectation that it would have robust and promiscuous activity. Strikingly, the catalytic domain did not have any appreciable histone methyltransferase activity, suggesting that the entire assembly is necessary. *Xl*MEP50 added to the catalytic domain reaction did not stimulate activity, as expected because MEP50 only binds to the missing PRMT5 N-terminal domain. The catalytic domain alone does not dimerize due to the head-to-tail arrangement of PRMT5.

Human and *Xenopus laevis* PRMT5 are highly homologous; as we previously showed, *Hs*PRMT5 methyltransferase activity is stimulated by *Xl*MEP50 (22). Here, we demonstrated that *Hs*PRMT5 does have very modest histone methyltransferase activity, with a signal on the fluorogram appearing after a year of film exposure, compared to the significantly stronger activity observed after addition of MEP50. Using our continuous luciferase-coupled assay we did not observe any activity above background for *Hs*PRMT5, so we are unable to assign kinetic parameters. *Xl*MEP50 addition also gave a quantitative increase in methyltransferase activity when titrated into the assay, consistent with multiple active PRMT5 molecules within the tetramer.

Substantial support for the role of MEP50 in histone recognition and catalysis by PRMT5 was provided by our continuous coupled assay. In agreement with Wang et. al. (43), we show that the K_m for *Ce*PRMT5 methylation of H4 tail peptide is about 650 times higher than that observed for *Xl*PRMT5-MEP50, and the catalytic efficiency for this peptide (~150 $M^{-1}s^{-1}$) is

roughly equivalent to the loss of efficiency we observe upon mutation of residue R42 from *Xl*MEP50 insertion loop (~45- 75-fold). These observations that protein substrate binding, represented by substrate K_m, is strongly dependent on the presence of MEP50 provide significant support for our hypothesis that MEP50 organizes substrate for PRMT5. Furthermore, the H4(1-7) short peptide would not be anticipated to be bound by MEP50 and therefore it should be poorly methylated by *Xl*PRMT5-MEP50. Indeed that is what we observed, as this very short peptide exhibited a 184 μM K_m, the highest value among all substrates assayed.

The MEP50-histone fold interaction orients the substrate for methylation— Competition studies between H2A and full length histone/peptide H4 clearly highlighted the importance of histone-fold domain for substrate recognition by PRMT5-MEP50. Intriguingly, the binding region for histone H2A may strongly overlap with some binding sites for histone H4, thus inhibiting methyltransfer onto H2AR3. However H3 is unable to fully abrogate the formation of H2A R3me1, so histones H2A and H3 may only share partial binding sites on the PRMT5-MEP50 complex. According to the strong competitive effects observed for both histone H3 and H4, the more physiologically relevant H3/H4 complex may be a substrate for *Xl*PRMT5-MEP50 under specific, yet undetermined, experimental conditions.

Our histone peptide array studies are also consistent with the PRMT5-MEP50 preference for binding that we observed for full-length H3 and H4 compared to H2A. Binding studies on these ultra-high density arrays will be generally useful for probing mechanisms of histone recognition by all histone acting enzymes. Furthermore, our quantitative determination of binding affinity between full-length H2A and *Xl*PRMT5-MEP50 (K_d = 1.78 ± 0.06 μM; Figure 3H) is in good agreement with peptide array and kinetic results in which H2A histone tail accounts for most of the binding onto the enzyme complex.

Recent publications have used kinetic and mass spectrometry analysis to model the reaction mechanism of PRMT5 and mutated PRMT1 in the generation of mono- and symmetric dimethylarginine (43,44,47). We independently confirmed this distributive model of progression to dimethylation through our demonstration that a synthesized monomethylated histone peptide has a 15-fold higher K_m than its equivalent unmethylated peptide. We did not observe any substantive difference in the k_{cat} between these two peptide substrates; these observations are likely incompatible with processive methylation and are therefore consistent with Wang et. al.'s observations of a distributive mode of progression to dimethylation with *Ce*PRMT5 on monomethylated substrates (43). Furthermore, our highly specific R3me1 and R3me2s antibodies confirmed that the dimethylation state did not appear until saturating levels of R3me1 (Figure 6D). Overall, these data and our prior observations of monomethylarginine *in vivo* point to the likely significant, but unexplored, biological role of monomethylation. Future studies will be needed to identify this biological role and potential monomethylarginine effector proteins.

PRMT5-MEP50 exhibits specific histone binding and methyltransfer— An enigma in the PRMT5 literature is that histone H3 and nucleosomal H4 substrates are well documented to be methylated by PRMT5 *in vivo* (40,41,48,49), yet H3 is not a substrate *in vitro*. Here, we confirmed that PRMT5-MEP50 does not methylate histones in recombinant nucleosomes. The results of our histone-peptide array study, and the mapping of the primary interaction domain to the his-

tone fold of H3 and H4, are entirely consistent with PRMT5's inability to methylate nucleosomes and provided an example of a novel use of these arrays. Crosstalk from other PTMs may explain this discrepancy, as suggested by observations showing that lysine acetylation stimulates PRMT5-MEP50 activity (50). Histones acetylated or otherwise modified *in vivo* may loosen histone:DNA contacts and may allow enough interaction to promote PRMT5 activity. We previously tested the enzyme complex's ability to methylate HeLa or hyperacetylated HeLa nucleosomes, but it was still unable to methylate these modified nucleosomes. Alternatively, other documented PRMT5 protein cofactors, such as COPR5 (15), Menin/Men1 (16), RioK1 (12), or ATP-dependent remodeling factors (18) may promote nucleosomal activity.

The MEP50 insertion finger is critical for the complex's substrate binding and activity- The MEP50 insertion finger directed over the cross-dimer PRMT5 catalytic domain is the WD40 repeat protein's most unique feature. We previously hypothesized that this insertion finger participates in organizing substrate for catalysis; alternatively, it may function to allosterically activate the PRMT5 catalytic domain, possibly mediated through the putative salt-bridge between MEP50R42 and PRMT5E403. Our mutagenesis of MEP50R42 to glutamic acid led to a dramatic loss of catalytic efficiency for both SAM and peptide substrates with the reversal of charge (R42E). However, we observed a different behavior of the more conservative $MEP50_{R42Q}$ complex, with kinetic parameters for SAM substrate nearly identical to those of the wild-type *Xl*PRMT5-MEP50. This loss of activity in the R42E mutant was primarily observed in a higher K_m, with only modest k_{cat} effects (32-40% of wildtype k_{cat}; Figure 6C), consistent with our hypothesis that histone/peptide substrate binding is dictated by MEP50 through intact positioning of the insertion finger. To our surprise, the K_m for SAM substrate (directly bound to C-term PRMT5 active site) was ~8-fold higher upon R42E mutation, suggesting that MEP50 may indeed have some small but direct influence on catalysis, possibly mediated through the putative salt bridge to the PRMT5 catalytic domain.

RbAp46, a WD-repeat protein and MEP50 analog that participates in multiple histone acetyltransferase complexes, was shown to bind histone H4 on its side face, as in our model for MEP50 binding (25). RbAp46 residues involved in H4 binding were isostructural with our predicted histone interaction domain on MEP50, providing convergent evolutionary support for our hypothesis. Furthermore, the H4 residues involved in binding RbAp46 were in the α1 helix of the histone fold (residues 24-41), consistent with the peptide array binding studies and providing support for the necessity of the histone fold interactions in the increased efficiency of full length histone substrate methylation by PRMT5-MEP50.

We combined all of our direct observations and propose the model shown in Figure 9. MEP50 is a presenter that 1) binds histones through their histone-fold domain 2) orients histone tail substrates toward PRMT5 cross-dimer active site for efficient arginine methylation. We anticipate that this model will guide studies on other histone methyltransferase complexes as well as provide insight for future drug design.

ACKNOWLEDGEMENTS

This work was supported by startup funds from the Albert Einstein College of Medicine, an Alexander and Alexandrine Sinsheimer Foundation Scholar Award, by The American Cancer Society – Robbie Sue Mudd Kidney Cancer Research Scholar Grant (124891-RSG-13-396-01-DMC) and NIH R01GM108646-01A1 (all to D.S.). We thank Dr. Michael Brenowitz for assistance with analytical ultracentrifugation studies. We are grateful to the New York Structural Genomics Research Consortium and the Einstein Macromolecular Therapeutics Development Facility for baculovirus production. U.R. and J.S. are employees of JPT Peptide Technologies. The peptide array used in this study has been developed and manufactured by JPT. The library on this array has been extended and is marketed as "Histone Code Peptide Microarray" (His-MA_01) by JPT.

REFERENCES

1. Di Lorenzo, A., and Bedford, M. T. (2011) Histone arginine methylation. *FEBS Lett* **585**, 2024-2031

2. Wolf, S. S. (2009) The protein arginine methyltransferase family: an update about function, new perspectives and the physiological role in humans. *Cell Mol Life Sci* **66**, 2109-2121

3. Wysocka, J., Allis, C. D., and Coonrod, S. (2006) Histone arginine methylation and its dynamic regulation. *Front Biosci* **11**, 344-355

4. Lee, Y. H., and Stallcup, M. R. (2009) Minireview: protein arginine methylation of nonhistone proteins in transcriptional regulation. *Mol Endocrinol* **23**, 425-433

5. Wilczek, C., Chitta, R., Woo, E., Shabanowitz, J., Chait, B. T., Hunt, D. F., and Shechter, D. (2011) Protein Arginine Methyltransferase Prmt5-Mep50 Methylates Histones H2A and H4 and the Histone Chaperone Nucleoplasmin in Xenopus laevis Eggs. *Journal of Biological Chemistry* **286**, 42221-42231

6. Bezzi, M., Teo, S. X., Muller, J., Mok, W. C., Sahu, S. K., Vardy, L. A., Bonday, Z. Q., and Guccione, E. (2013) Regulation of constitutive and alternative splicing by PRMT5 reveals a role for Mdm4 pre-mRNA in sensing defects in the spliceosomal machinery. *Genes Dev* **27**, 1903-1916

7. Scoumanne, A., Zhang, J., and Chen, X. (2009) PRMT5 is required for cell-cycle progression and p53 tumor suppressor function. *Nucleic Acids Res* **37**, 4965-4976

8. Friesen, W. J., Wyce, A., Paushkin, S., Abel, L., Rappsilber, J., Mann, M., and Dreyfuss, G. (2002) A novel WD repeat protein component of the methylosome binds Sm proteins. *J Biol Chem* **277**, 8243-8247

9. Furuno, K., Masatsugu, T., Sonoda, M., Sasazuki, T., and Yamamoto, K. (2006) Association of Polycomb group SUZ12 with WD-repeat protein MEP50 that binds to histone H2A selectively in vitro. *Biochem Biophys Res Commun* **345**, 1051-1058

10. Le Guezennec, X., Vermeulen, M., Brinkman, A. B., Hoeijmakers, W. A., Cohen, A., Lasonder, E., and Stunnenberg, H. G. (2006) MBD2/NuRD and MBD3/NuRD, two distinct complexes with different biochemical and functional properties. *Mol Cell Biol* **26**, 843-851

11. Aggarwal, P., Vaites, L. P., Kim, J. K., Mellert, H., Gurung, B., Nakagawa, H., Herlyn, M., Hua, X., Rustgi, A. K., McMahon, S. B., and Diehl, J. A. (2010) Nuclear cyclin D1/CDK4 kinase

regulates CUL4 expression and triggers neoplastic growth via activation of the PRMT5 methyltransferase. *Cancer Cell* **18**, 329-340

12. Guderian, G., Peter, C., Wiesner, J., Sickmann, A., Schulze-Osthoff, K., Fischer, U., and Grimmler, M. (2011) RioK1, a new interactor of protein arginine methyltransferase 5 (PRMT5), competes with pICln for binding and modulates PRMT5 complex composition and substrate specificity. *J Biol Chem* **286**, 1976-1986

13. Ancelin, K., Lange, U. C., Hajkova, P., Schneider, R., Bannister, A. J., Kouzarides, T., and Surani, M. A. (2006) Blimp1 associates with Prmt5 and directs histone arginine methylation in mouse germ cells. *Nat Cell Biol* **8**, 623-630

14. Friesen, W. J., Paushkin, S., Wyce, A., Massenet, S., Pesiridis, G. S., Van Duyne, G., Rappsilber, J., Mann, M., and Dreyfuss, G. (2001) The methylosome, a 20S complex containing JBP1 and pICln, produces dimethylarginine-modified Sm proteins. *Mol Cell Biol* **21**, 8289-8300

15. Lacroix, M., Messaoudi, S. E., Rodier, G., Le Cam, A., Sardet, C., and Fabbrizio, E. (2008) The histone-binding protein COPR5 is required for nuclear functions of the protein arginine methyltransferase PRMT5. *EMBO reports* **9**, 452-458

16. Gurung, B., Feng, Z., Iwamoto, D. V., Thiel, A., Jin, G., Fan, C. M., Ng, J. M., Curran, T., and Hua, X. (2013) Menin epigenetically represses Hedgehog signaling in MEN1 tumor syndrome. *Cancer Res* **73**, 2650-2658

17. Karkhanis, V., Hu, Y.-J., Baiocchi, R. A., Imbalzano, A. N., and Sif, S. (2011) Versatility of PRMT5-induced methylation in growth control and development. *Trends in Biochemical Sciences* **36**, 633-641

18. Pal, S., Vishwanath, S. N., Erdjument-Bromage, H., Tempst, P., and Sif, S. (2004) Human SWI/SNF-associated PRMT5 methylates histone H3 arginine 8 and negatively regulates expression of ST7 and NM23 tumor suppressor genes. *Mol Cell Biol* **24**, 9630-9645

19. Yan, F., Alinari, L., Lustberg, M. E., Katherine Martin, L., Cordero-Nieves, H. M., Banasavadi-Siddegowda, Y., Virk, S., Barnholtz-Sloan, J., Bell, E. H., Wojton, J., Jacob, N. K., Chakravarti, A., Nowicki, M. O., Wu, X., Lapalombella, R., Datta, J., Yu, B., Gordon, K., Haseley, A., Patton, J. T., Smith, P. L., Ryu, J., Zhang, X., Mo, X., Marcucci, G., Nuovo, G., Kwon, C. H., Byrd, J. C., Chiocca, E. A., Li, C., Sif, S., Jacob, S., Lawler, S., Kaur, B., and Baiocchi, R. A. (2014) Genetic Validation of the Protein Arginine Methyltransferase PRMT5 as a Candidate Therapeutic Target in Glioblastoma. *Cancer Res* **74**, 1752-1765

20. Bao, X., Zhao, S., Liu, T., Liu, Y., Liu, Y., and Yang, X. (2013) Overexpression of PRMT5 promotes tumor cell growth and is associated with poor disease prognosis in epithelial ovarian cancer. *J Histochem Cytochem* **61**, 206-217

21. Gu, Z., Gao, S., Zhang, F., Wang, Z., Ma, W., Davis, R. E., and Wang, Z. (2012) Protein arginine methyltransferase 5 is essential for growth of lung cancer cells. *Biochem J* **446**, 235-241

22. Ho, M.-C., Wilczek, C., Bonanno, J. B., Xing, L., Seznec, J., Matsui, T., Carter, L. G., Onikubo, T., Kumar, P. R., Chan, M. K., Brenowitz, M., Cheng, R. H., Reimer, U., Almo, S. C., and Shechter, D. (2013) Structure of the Arginine Methyltransferase PRMT5-MEP50 Reveals a Mechanism for Substrate Specificity. *PLoS ONE* **8**, e57008

23. Antonysamy, S., Bonday, Z., Campbell, R. M., Doyle, B., Druzina, Z., Gheyi, T., Han, B., Jungheim, L. N., Qian, Y., Rauch, C., Russell, M., Sauder, J. M., Wasserman, S. R., Weichert, K., Willard, F. S., Zhang, A., and Emtage, S. (2012) Crystal structure of the human PRMT5:MEP50 complex. *Proceedings of the National Academy of Sciences of the United States of America* **109**, 17960-17965

24. Ruthenburg, A. J., Wang, W., Graybosch, D. M., Li, H., Allis, C. D., Patel, D. J., and Verdine, G. L. (2006) Histone H3 recognition and presentation by the WDR5 module of the MLL1 complex. *Nat Struct Mol Biol* **13**, 704-712

25. Murzina, N. V., Pei, X. Y., Zhang, W., Sparkes, M., Vicente-Garcia, J., Pratap, J. V., McLaughlin, S. H., Ben-Shahar, T. R., Verreault, A., Luisi, B. F., and Laue, E. D. (2008) Structural basis for the recognition of histone H4 by the histone-chaperone RbAp46. *Structure* **16**, 1077-1085

26. Hemeon, I., Gutierrez, J. A., Ho, M. C., and Schramm, V. L. (2011) Characterizing DNA methyltransferases with an ultrasensitive luciferase-linked continuous assay. *Anal Chem* **83**, 4996-5004

27. Sturm, M. B., and Schramm, V. L. (2009) Detecting ricin: sensitive luminescent assay for ricin A-chain ribosome depurination kinetics. *Analytical chemistry* **81**, 2847-2853

28. Wang, H. C., Ciskanik, L., Dunaway-Mariano, D., von der Saal, W., and Villafranca, J. J. (1988) Investigations of the partial reactions catalyzed by pyruvate phosphate dikinase. *Biochemistry* **27**, 625-633

29. Morrison, J. F. (1969) Kinetics of the reversible inhibition of enzyme-catalysed reactions by tight-binding inhibitors. *Biochimica et biophysica acta* **185**, 269-286

30. Humphrey, W., Dalke, A., and Schulten, K. (1996) VMD: visual molecular dynamics. *J Mol Graph* **14**, 33-38, 27-38

31. Russell, R. B., and Barton, G. J. (1992) Multiple protein sequence alignment from tertiary structure comparison: assignment of global and residue confidence levels. *Proteins* **14**, 309-323

32. Roberts, E., Eargle, J., Wright, D., and Luthey-Schulten, Z. (2006) MultiSeq: unifying sequence and structure data for evolutionary analysis. *BMC Bioinformatics* **7**, 382

33. Comeau, S. R., Gatchell, D. W., Vajda, S., and Camacho, C. J. (2004) ClusPro: a fully automated algorithm for protein-protein docking. *Nucleic Acids Res* **32**, W96-99

34. Comeau, S. R., Gatchell, D. W., Vajda, S., and Camacho, C. J. (2004) ClusPro: an automated docking and discrimination method for the prediction of protein complexes. *Bioinformatics* **20**, 45-50

35. Shechter, D., Nicklay, J. J., Chitta, R. K., Shabanowitz, J., Hunt, D. F., and Allis, C. D. (2009) Analysis of histones in Xenopus laevis. I. A distinct index of enriched variants and modifications exists in each cell type and is remodeled during developmental transitions. *J Biol Chem* **284**, 1064-1074

36. Nicklay, J. J., Shechter, D., Chitta, R. K., Garcia, B. A., Shabanowitz, J., Allis, C. D., and Hunt, D. F. (2009) Analysis of histones in Xenopus laevis. II. mass spectrometry reveals an index of cell type-specific modifications on H3 and H4. *J Biol Chem* **284**, 1075-1085

37. Tee, W. W., Pardo, M., Theunissen, T. W., Yu, L., Choudhary, J. S., Hajkova, P., and Surani, M. A. (2010) Prmt5 is essential for early mouse development and acts in the cytoplasm to maintain ES cell pluripotency. *Genes Dev* **24**, 2772-2777

38. Shechter, D., Dormann, H. L., Allis, C. D., and Hake, S. B. (2007) Extraction, purification and analysis of histones. *Nature protocols* **2**, 1445-1457

39. Fabbrizio, E., El Messaoudi, S., Polanowska, J., Paul, C., Cook, J. R., Lee, J. H., Negre, V., Rousset, M., Pestka, S., Le Cam, A., and Sardet, C. (2002) Negative regulation of transcription by the type II arginine methyltransferase PRMT5. *EMBO reports* **3**, 641-645

40. Majumder, S., Alinari, L., Roy, S., Miller, T., Datta, J., Sif, S., Baiocchi, R., and Jacob, S. T. (2010) Methylation of histone H3 and H4 by PRMT5 regulates ribosomal RNA gene transcription. *J Cell Biochem* **109**, 553-563

41. Wang, L., Pal, S., and Sif, S. (2008) Protein arginine methyltransferase 5 suppresses the transcription of the RB family of tumor suppressors in leukemia and lymphoma cells. *Mol Cell Biol* **28**, 6262-6277

42. Wang, M., Fuhrmann, J., and Thompson, P. R. (2014) Protein arginine methyltransferase 5 catalyzes substrate dimethylation in a distributive fashion. *Biochemistry* **53**, 7884-7892

43. Wang, M., Xu, R. M., and Thompson, P. R. (2013) Substrate specificity, processivity, and kinetic mechanism of protein arginine methyltransferase 5. *Biochemistry* **52**, 5430-5440

44. Gui, S., Gathiaka, S., Li, J., Qu, J., Acevedo, O., and Hevel, J. M. (2014) A remodeled protein arginine methyltransferase 1 (PRMT1) generates symmetric dimethylarginine. *J Biol Chem* **289**, 9320-9327

45. Porollo, A., and Meller, J. (2007) Prediction-based fingerprints of protein-protein interactions. *Proteins* **66**, 630-645

46. Zhang, Q. C., Deng, L., Fisher, M., Guan, J., Honig, B., and Petrey, D. (2011) PredUs: a web server for predicting protein interfaces using structural neighbors. *Nucleic Acids Res* **39**, W283-287

47. Wang, W.-L., Anderson, L., Nicklay, J., Chen, H., Gamble, M., Shabanowitz, J., Hunt, D., and Shechter, D. (2014) Phosphorylation and arginine methylation mark histone H2A prior to deposition during Xenopus laevis development. *Epigenetics & Chromatin* **7**, 22

48. Zhao, Q., Rank, G., Tan, Y. T., Li, H., Moritz, R. L., Simpson, R. J., Cerruti, L., Curtis, D. J., Patel, D. J., Allis, C. D., Cunningham, J. M., and Jane, S. M. (2009) PRMT5-mediated methylation of histone H4R3 recruits DNMT3A, coupling histone and DNA methylation in gene silencing. *Nat Struct Mol Biol* **16**, 304-311

49. Pal, S., Baiocchi, R. A., Byrd, J. C., Grever, M. R., Jacob, S. T., and Sif, S. (2007) Low levels of miR-92b/96 induce PRMT5 translation and H3R8/H4R3 methylation in mantle cell lymphoma. *The EMBO journal* **26**, 3558-3569

50. Feng, Y., Wang, J., Asher, S., Hoang, L., Guardiani, C., Ivanov, I., and Zheng, Y. G. (2011) Histone H4 Acetylation Differentially Modulates Arginine Methylation by an in Cis Mechanism. *Journal of Biological Chemistry* **286**, 20323-20334

FIGURE LEGENDS

Figure 1. *Evolutionarily conserved spatial arrangement between the PRMT5 catalytic domain and its cross-dimer paired MEP50.* **A.** Ribbon diagram of the *Xenopus* PRMT5 monomer (purple), its directly bound MEP50 molecule (pink), and the cross-dimer MEP50 (blue). Structural alignment windows 1, 2, and 3 are indicated on the right. Insert boxes: surface diagrams of the *Xenopus* (PDB:4G56) and human (PDB:4GQB) PRMT5-MEP50 structures, with the analyzed PRMT5 and MEP50 molecules colored as in A, the remainder of the structures are shown in gray. **B.** Per-residue Cα alignments between the *Xenopus* and human PRMT5 windows 1,2, and 3 as calculated with VMD MultiSeq, plotted as root-mean-square deviation (RMSD; Å) against amino acid position in the sequence. The PRMT5 alignment windows are boxed.

Figure 2. *Intact full-length PRMT5 complexed with MEP50 is necessary for histone methyltransferase activity.* **A.** The catalytic C-terminal domain of *Xl*PRMT5 (residues 291-633) is shown in purple and was expressed and purified. **B.** *Xl*PRMT5(291-633) did not exhibit any activity towards histone tail peptide substrates of the intact complex [H2A(1-20), H4(1-20), H4(1-7)] or full length histones H2A or H4. Addition of *Xl*MEP50 to the catalytic domain did not stimulate activity, while addition of *Xl*MEP50 to full-length *Hs*PRMT5 stimulated activity towards H2A(1-20) peptide. **C.** Intact *Xl*PRMT5-MEP50 complex, or *Hs*PRMT5 + *Xl*MEP50, exhibited methyltransferase activity towards histone H4 (right two lanes). *Hs*PRMT5 alone exhibited ultra-low levels of activity towards H2A, H3, and H4, visible only after a one-year exposure of the fluorogram (left four lanes, second panel). **D.** *Hs*PRMT5 (200 nM) was pre-incubated with sub-stoichiometric (1:4, 2:4) and stoichiometric concentrations (4:4) of *Xl*MEP50 and then assayed for methyltransferase activity against H4 peptide.

Figure 3. *XlMEP50 is a presenter that primarily binds histone H4 through the histone fold and exposes its N-terminal tail for methylation by XlPRMT5.* **A.** Substrate competition experiment where *Xl*PRMT5-MEP50 activity towards histone H2A was displaced as histone H4 was titrated into the reaction (experiment performed using 50 mM MOPS pH 7.0, 100 nM *Xl*PRMT5-MEP50 and 20 μU of *Se*MTAN, 25 μM [^{14}C]-methyl-SAM, a H2A concentration kept constant at 2 μM, while H4 was added at 0, 0.4, 0.8, 1.6, 3.2, 6.4 and 12.8 μM final concentrations). **B.** Similar competition experiment as in A where peptide H4(1-20) was used as competing substrate (experimental conditions identical as in A). **C.** Quantification of methyltransfer reactions using reversed-phase HPLC. Histones H4, H2A, tailless H2A (TLH2A) and H3 were separated from each other and from radiolabelled substrate SAM using a C_8 reverse HPLC column (see experimental procedures). **D.** Substrate competition experiment where *Xl*PRMT5-MEP50 activity towards histone H2A was displaced as histone H4, peptide H4(1-20) and histone H3 were titrated into the reaction (experiment performed using 50 mM MOPS pH 7.0, 100 nM *Xl*PRMT5-MEP50 and 20 μU of *Se*MTAN, 25 μM [^{3}H]-methyl-SAM, a H2A concentration kept constant at 2 μM, while competitors were added at 0-12.6 μM final concentrations). Transfer of [^{3}H]-methyl was quantified by liquid scintillation counting after isolation of histones. **E.** Similar competition experiment as in D where *Xl*PRMT5-MEP50 was replaced by its homologous enzyme from *C. elegans* (experimental conditions identical as in D). **F.** Flag-*Hs*PRMT5-*Xl*MEP50 complex was incubated on ultra-high density histone peptide arrays. PRMT5-MEP50 binding on the histone peptide scan data was extracted and relative binding levels were plotted as a heatmap, with no-to-low signal as white to

light yellow, and high relative binding was plotted in red. Histone amino-acid sequence numbers are represented on the top of the plots. The histone-fold domain is indicated as a gray box and the substrate residue R3 on both H2A and H4 is annotated. **G.** Relief of methyltransferase activity through addition of MEP50. In this model used to determine the affinities of histone H2A for MEP50, $P/M^{*}\bullet H$ represents the PRMT5-MEP50●Histone complex where only the histone fold is bound to the MEP50 presenter. $P^{*}/M^{*}\bullet H$ represents the PRMT5-MEP50●Histone complex where the histone fold is bound to the MEP50 presenter and the histone tail is bound to the enzyme active site. $M^{*}\bullet H$ represents the complex between histone and exogenous MEP50. Each step is characterized by a constant (i.e. k_1, k_{-1}, k_2, k_{-2}, k_{cat}, k_3 and k_{-3}). **G.** Transferase reaction catalyzed by *Xl*PRMT5-MEP50 was followed continuously at pH 7.7 using the luciferase-based assay with histone H2A as substrate (H2A fixed at 2 μM; see experimental procedures); *Xl*MEP50 was added to the reactions (0-20 μM) and resulting transferase activities were recorded. Exogenous *Xl*MEP50 competes with *Xl*PRMT5-MEP50 for H2A binding and methyltransfer is inhibited with increasing concentrations of *Xl*MEP50. A dissociation constant (K_d) of H2A for both exogenous *Xl*MEP50 (K_d´ H2A:MEP50) and PRMT5-associated MEP50 (K_d H2A:complex) was determined.

Figure 4. *XlPRMT5-MEP50 does not methylate histones embedded in DNA in nucleosomes.* **A.** *Xl*PRMT5-MEP50 was incubated with H2A, H4, or recombinant mononucleosomes, in the presence or absence of DNase I. PRMT5 methylated both H2A and H4 independently (lanes 1 and 2) but did not methylate histones in mononucleosomes (lane 3). Upon DNase I treatment, histone H4 and histone H2A activity was recovered (lane 4). **B.** Cartoon representation of the nucleosome core particle (PDB:1KX5), with H3 shown in blue, H4 in green, H2A in red and H2B in yellow The targeted H4 R3 is shown (gray coloring and arrow) and the region on H3/H4 corresponding to the strongest sites of interaction on the peptide array is noted.

Figure 5. *Mutations of MEP50 insertion loop residue R42 affect histone methylation.* **A.** Cartoon representation of the insertion loop from the cross-dimer *Xl*MEP50 positioned adjacent to the catalytic domain of the paired PRMT5 molecular. Insert zoom view: The only contact the cross-dimer MEP50 makes with the catalytic domain is a putative salt bridge between *Xl*MEP50$_{R42}$ and *Xl*PRMT5$_{E403}$; no other contacting residues are found. **B.** Coomassie stained gel of wild-type *Xl*PRMT5-MEP50, *Xl*PRMT5-MEP50$_{R42E}$ and *Xl*PRMT5-MEP50$_{R42Q}$ complexes. **C.** Coomassie stained gel of wild-type and *Xl*MEP50$_{R42E}$. **D.** Flag-tagged *Hs*PRMT5 captured on anti-Flag resin after incubation alone, with *Xl*MEP50, *Xl*MEP50$_{R42E}$, or *Xl*MEP50$_{R42Q}$ and immunoblotted for *Hs*PRMT5 and *Xl*MEP50, demonstrating similar interactions for the wild-type and mutated MEP50 proteins. **E.** Filter-binding activity assays of PRMT5-MEP50, PRMT5-MEP50$_{R42E}$, or PRMT5-MEP50$_{R42Q}$ (100nM complex) incubated with H2A(1-20), H4(1-20) and Npm(177-196) substrate peptides or H2A and H4 full-length protein substrates. PRMT5 directed activity is represented as percent of wild-type activity towards the peptide/protein substrate and is the average of three independent replicates.

Figure 6. *Substrate specificities for XlPRMT5-MEP50 and the impact on enzymatic efficiency upon mutation of MEP50 insertion loop residue R42.* Kinetic parameters for the various tested substrates (histone H4, histone peptides and SAM) are plotted, with the k_{cat} (h^{-1}) on the y-axis and the K_m (nM; logarithmic scale) on the x-axis. Highest enzymatic efficiencies are obtained with

substrates found on the upper left quadrant while low enzymatic efficiencies are obtained with substrates found on the opposite lower right quadrant. Arrows indicate the loss (squared values) of enzymatic efficiency upon arginine monomethylation (purple) or upon mutation of MEP50 residue R42 to glutamic acid (red) and to glutamine (green). For reference, enzymatic behavior of *Ce*PRMT5 is represented in blue. **A.** Representation of kinetic parameters for histone substrates using saturating concentration of SAM. **B.** Representation of kinetic parameters for SAM substrate using saturating concentration of histone substrates. **C.** Impact of *Xl*MEP50$_{R42Q}$ and *Xl*MEP50$_{R42E}$ onto catalytic turn-over (k_{cat}; pink bars) and substrates' affinities (K_m; grey bars) for both peptide and SAM substrates. The decrease of methyltansfer is represented as a percentage of wild-type k_{cat} while the loss of affinity is given as fold increase of wild-type K_m. **D.** Histones H2A or H4 were incubated with *Xl*PRMT5-MEP50 and SAM. Reactions were stopped at 0, 1, 5, 10, and 15 minutes with the addition of SDS-PAGE gel loading buffer and heating to 100ºC. Reaction products were immunoblotted with monomethylarginine (R3me1) or symmetric dimethylarginine (R3me2s) specific antibodies.

Figure 7. *Prediction of histone binding sites onto the PRMT5-MEP50 complex.* **A.** The predicted interacting residues on the cross-dimer pair of *Xl*PRMT5-MEP50 was determined using the SPPIDER and PredUs algorithms and mapped onto the structure as shown in yellow. **B.** Docking of H2A/H2B dimer (orange/yellow) and **C.** H3/H4 dimer (blue/green) onto *Xl*PRMT5-MEP50 [PRMT5 monomer (purple), its directly bound MEP50 molecule (pink), and the cross-dimer MEP50 (blue)], using ClusPro with attractive forces as determined by the peptide array and predictions in A.

Figure 8. *Schematic model for the sequential binding of core histone onto the MEP50 presenter and favorable orientation of the N-terminal histone tail to the PRMT5 active site for methyltransfer.* *Xl*PRMT5-MEP50 is a tetramer of heterodimers and the cross-dimer MEP50 (green) is paired with its cognate PRMT5 molecule (grey; C-term active site represented by the symbol *) to promote histone methylation according to a sequential mechanism with **1**) binding of the full-length histone through its histone fold (*FL*H in red; dissociation constant K_d), **2**) favorable orientation of the histone tail toward the PRMT5 cross-dimer active site (symbol *; step characterized by a K_m value), **3**) methylation of the arginine R3 (yellow circle with methyl group transferred from *S*-adenosyl methionine; step characterized by a k_{cat} value), **4**) release of the methylated histone tail and the histone fold from the active site and the MEP50, respectively.

substrate	sequence	kinetic parameters		
		K_m (nM)[a]	k_{cat} (h^{-1})[a]	ξ ($M^{-1}.s^{-1}$)[b]
Histone H4				
Full length protein		211 ± 73	21 ± 2	2.8×10^4
H4 (1-7)	*H*-SGRGKGG-*OH*	(184 ± 20) x 10^3	32 ± 2	48
SAM		(4.7 ± 0.5) x 10^3	26.2 ± 0.6	1.5×10^3
H4 (1-7) PRMT5-MEP50^{R42E}		(515 ± 52) x 10^3	9.4 ± 0.3	5
SAM		(108 ± 31) x 10^3	10 ± 1	26
H4 (1-21)	*H*-SGRGKGGKGLGKGGAKRHRKV-*OH*	343 ± 42	36 ± 1	2.9×10^4
H4 (1-21)[c] *Hs*PRMT5-*Hs*MEP50	*Ac*-SGRGKGGKGLGKGGAKRHRKV	1600 ± 1000	10.8 ± 0.6	1.9×10^3
H4 (1-20)	*H*-SGRGKGGKGLGKGGAKRHRK-*OH*	83 ± 8	37.6 ± 0.9	1.3×10^5
SAM		(3.3 ± 0.2) x 10^3	27.4 ± 0.3	2.3×10^3
H4 (1-20) PRMT5-MEP50^{R42E}		(2.0 ± 0.2) x 10^3	12 ± 0.3	1.7×10^3
SAM		(27 ± 3) x 10^3	10.9 ± 0.4	112
H4 (1-20) PRMT5-MEP50^{R42Q}		502 ± 140	5.4 ± 0.4	3.0×10^3
SAM		(5.3 ± 0.5) x 10^3	5.7 ± 0.1	300
H4 (1-20)	*Ac*-SGRGKGGKGLGKGGAKRHRKK$^{(Biot)}$	139 ± 16	21.1 ± 0.6	4.2×10^4
H4 K12$^{(Ac)}$ (1-20)	*Ac*-SGRGKGGKGLGK$^{(Ac)}$GGAKRHRKK$^{(Biot)}$	195 ± 35	29 ± 1	3.7×10^4
H4 K20$^{(Me)2}$ (1-20)	*Ac*-SGRGKGGKGLGKGGAKRHRK$^{(Me)2}$K$^{(Biot)}$	124 ± 18	24.5 ± 0.8	5.5×10^4
H4 K12$^{(Ac)}$K20$^{(Me)2}$ (1-20)	*Ac*-SGRGKGGKGLGK$^{(Ac)}$GGAKRHRK$^{(Me)2}$K$^{(Biot)}$	279 ± 25	24.4 ± 0.7	2.4×10^4
H4 (1-20) *Ce*PRMT5	*H*-SGRGKGGKGLGKGGAKRHRK-*OH*	(54 ± 4) x 10^3	28.6 ± 0.7	150
SAM		(4.4 ± 0.8) x 10^3	32 ± 1	2.0×10^3
Histone H2A				
Hs H2A (1-20)	*H*-SGRGKQGGKARAKAKTRSSR-*OH*	867 ± 136	43 ± 3	1.4×10^4
Xl H2A.X-F (1-20)	*Ac*-SGRGKKVQKAASGKASRSAKA-CY-*OH*	(1.74 ± 0.09) x 10^3	51 ± 1	8.2×10^3
Xl H2A.X-F R3$^{(Me)}$ (1-20)	*Ac*-SGR$^{(Me)}$GKKVQKAASGKASRSAKA-CY-*OH*	(25 ± 2) x 10^3	40 ± 1	445
***Xl* Nucleoplasmin**				
Full length protein		(1.6 ± 0.2) x 10^3	28 ± 2	4.9×10^3

[a]Kinetic parameters obtained by fitting experimental values to the Morrison kinetic model (Equation 1); [b]Catalytic efficiency represented by $\xi = k_{cat}/K_m$; [c]From published study on *Hs*PRMT5-MEP50 (Ref. 42).

Table 1. Kinetic parameters for *Xenopus laevis (Xl)* PRMT5-MEP50, its MEP50 mutants, and *Caenorhabditis elegans* (*Ce)* PRMT5 (boxed). Parameters for the SAM substrate are below the corresponding peptide substrate.

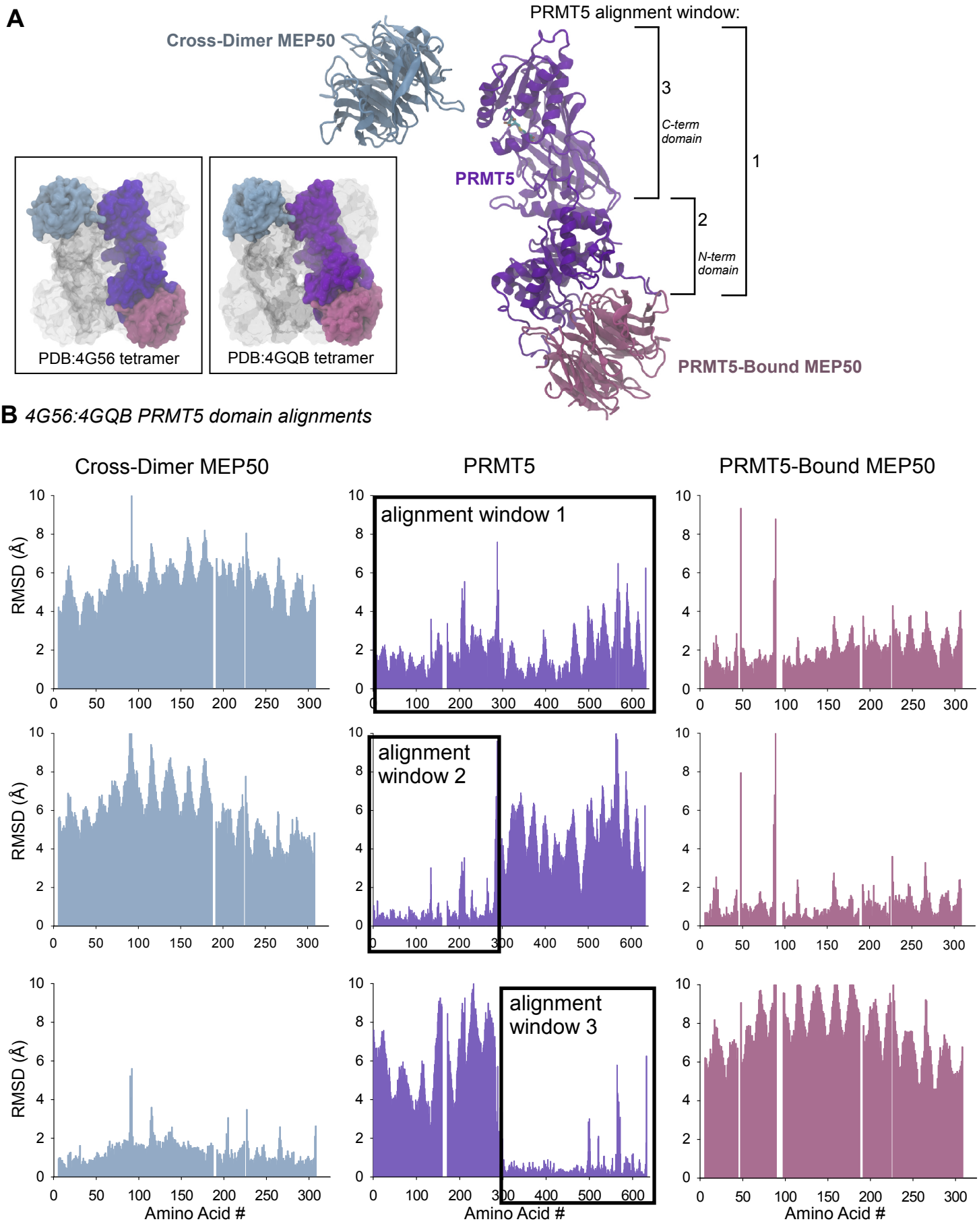

Figure 1

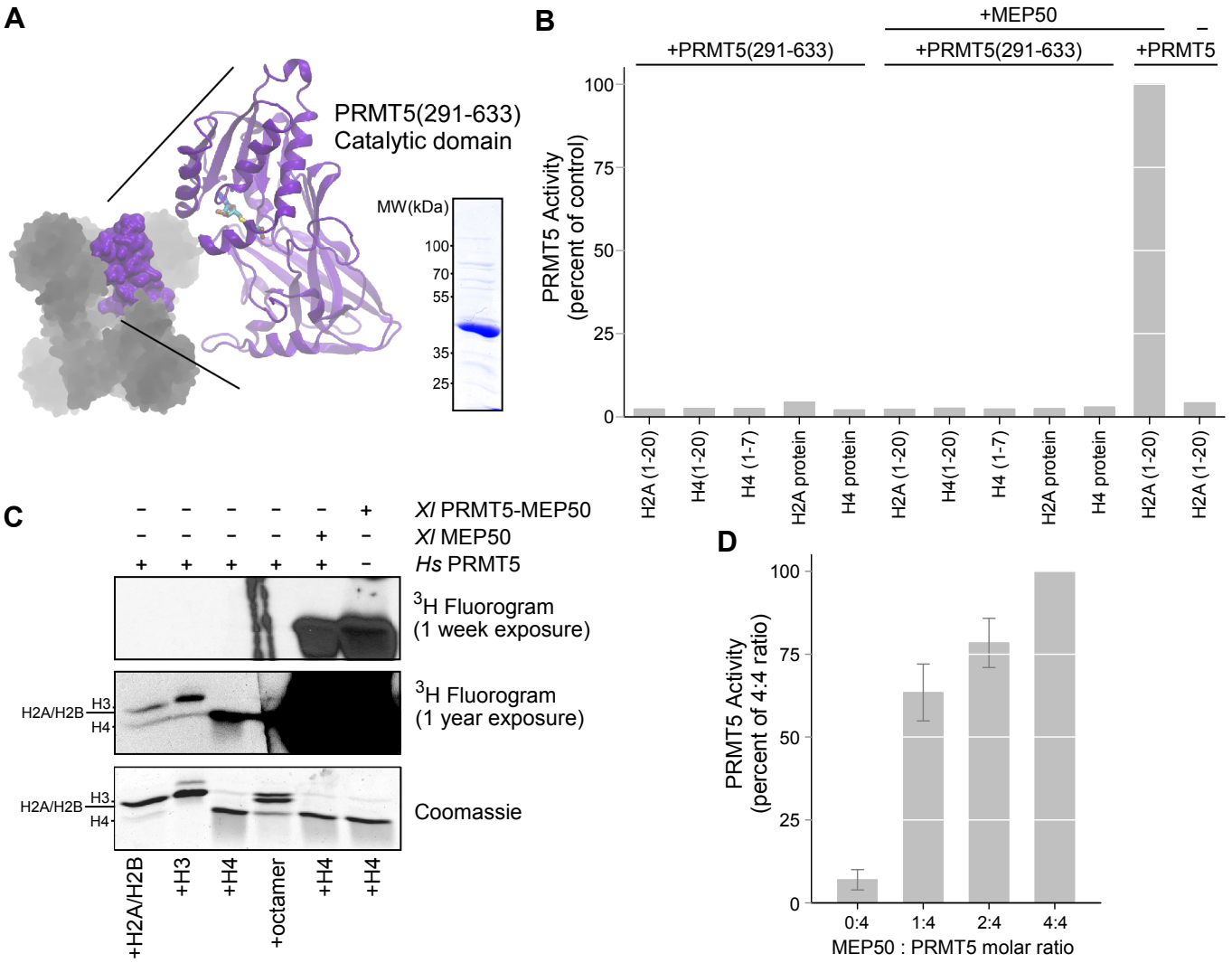

Figure 2

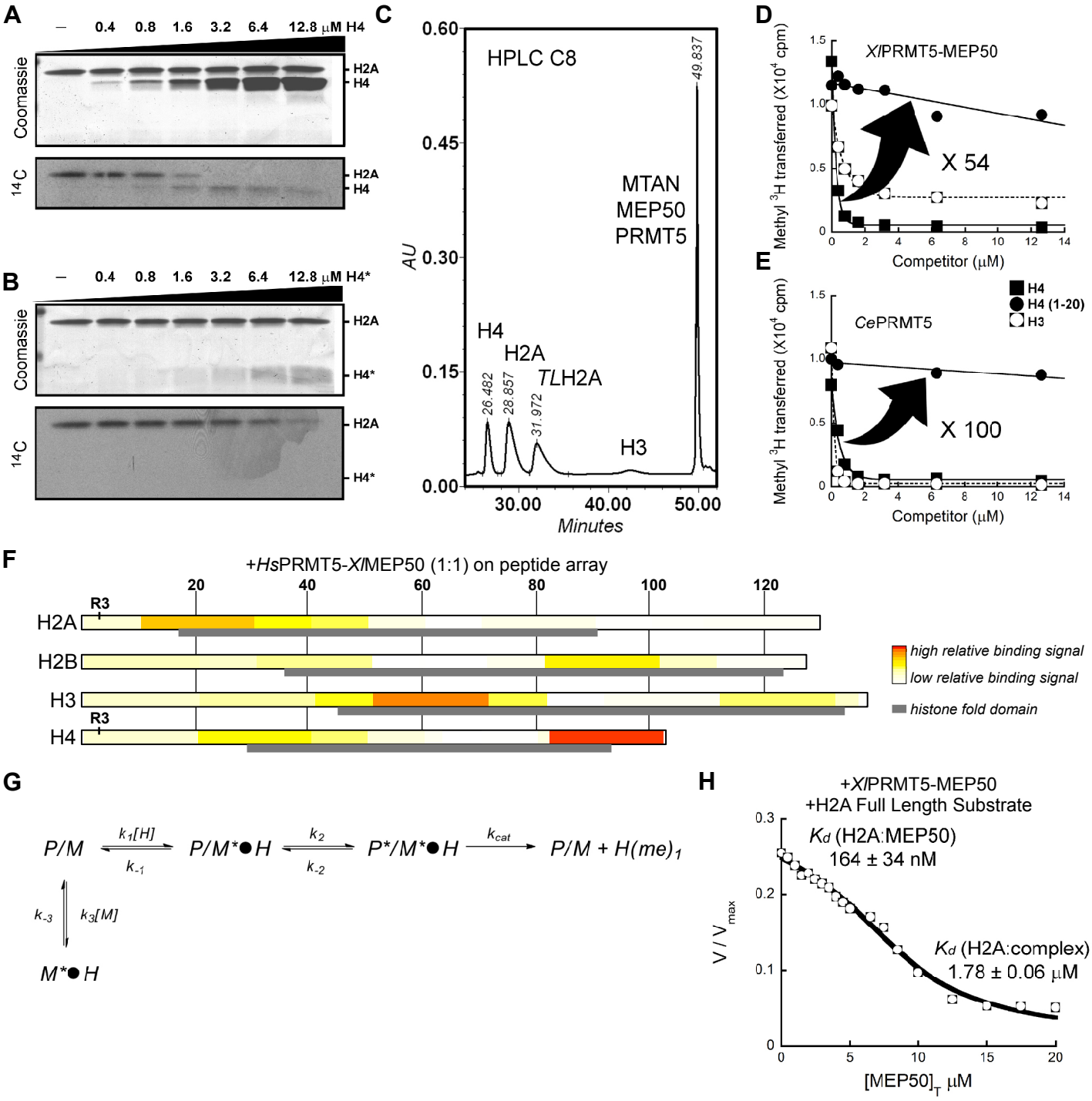

Figure 3

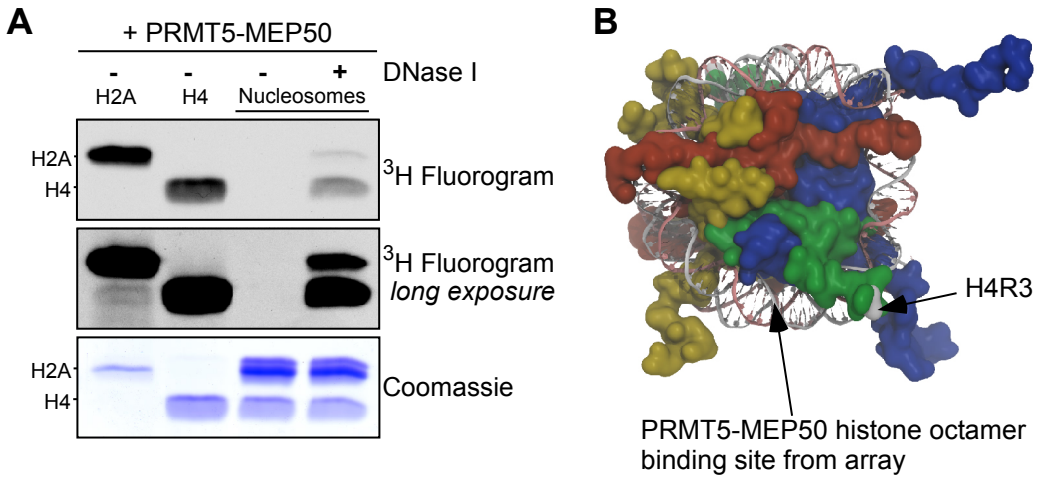

Figure 4

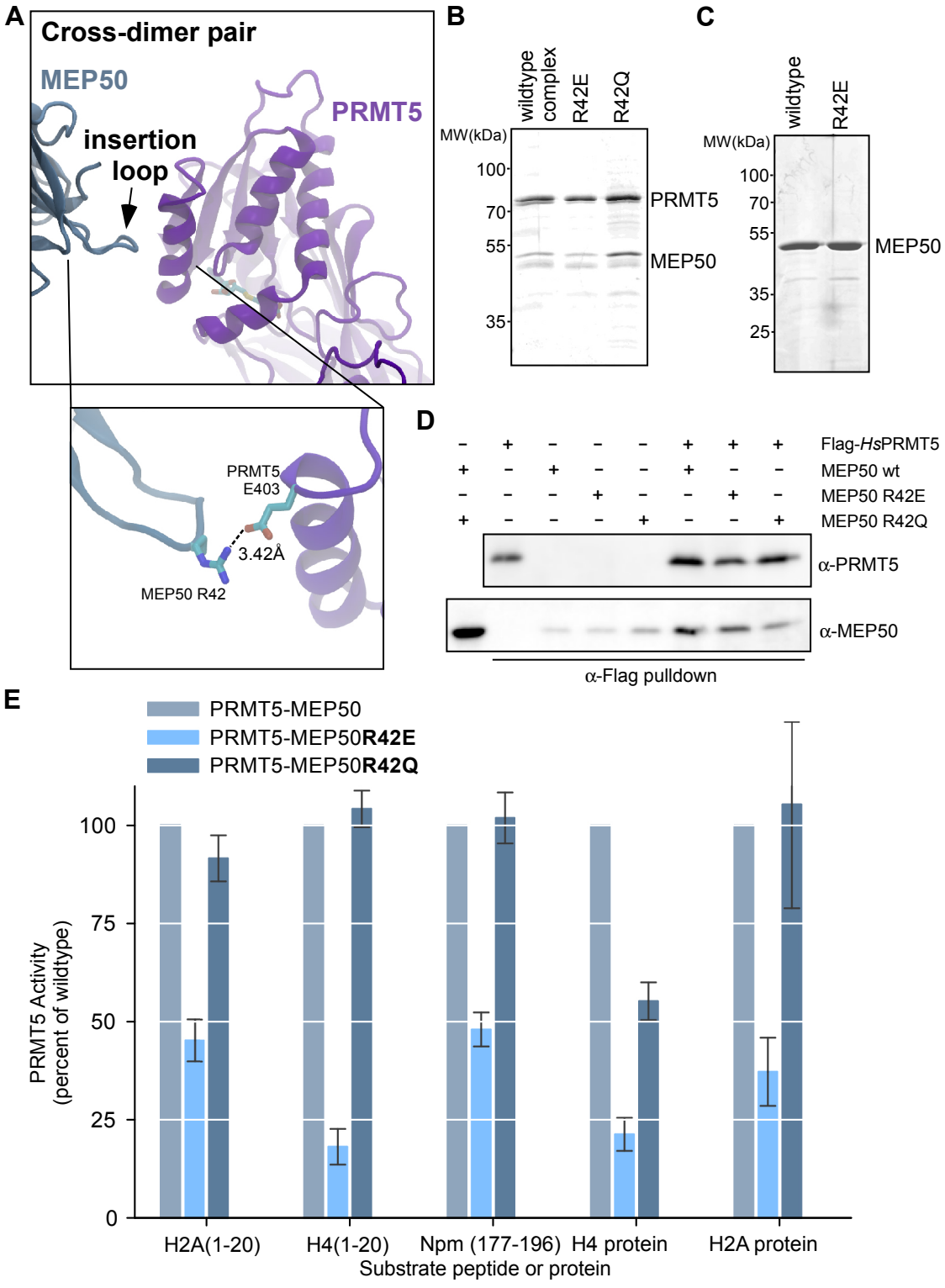

Figure 5

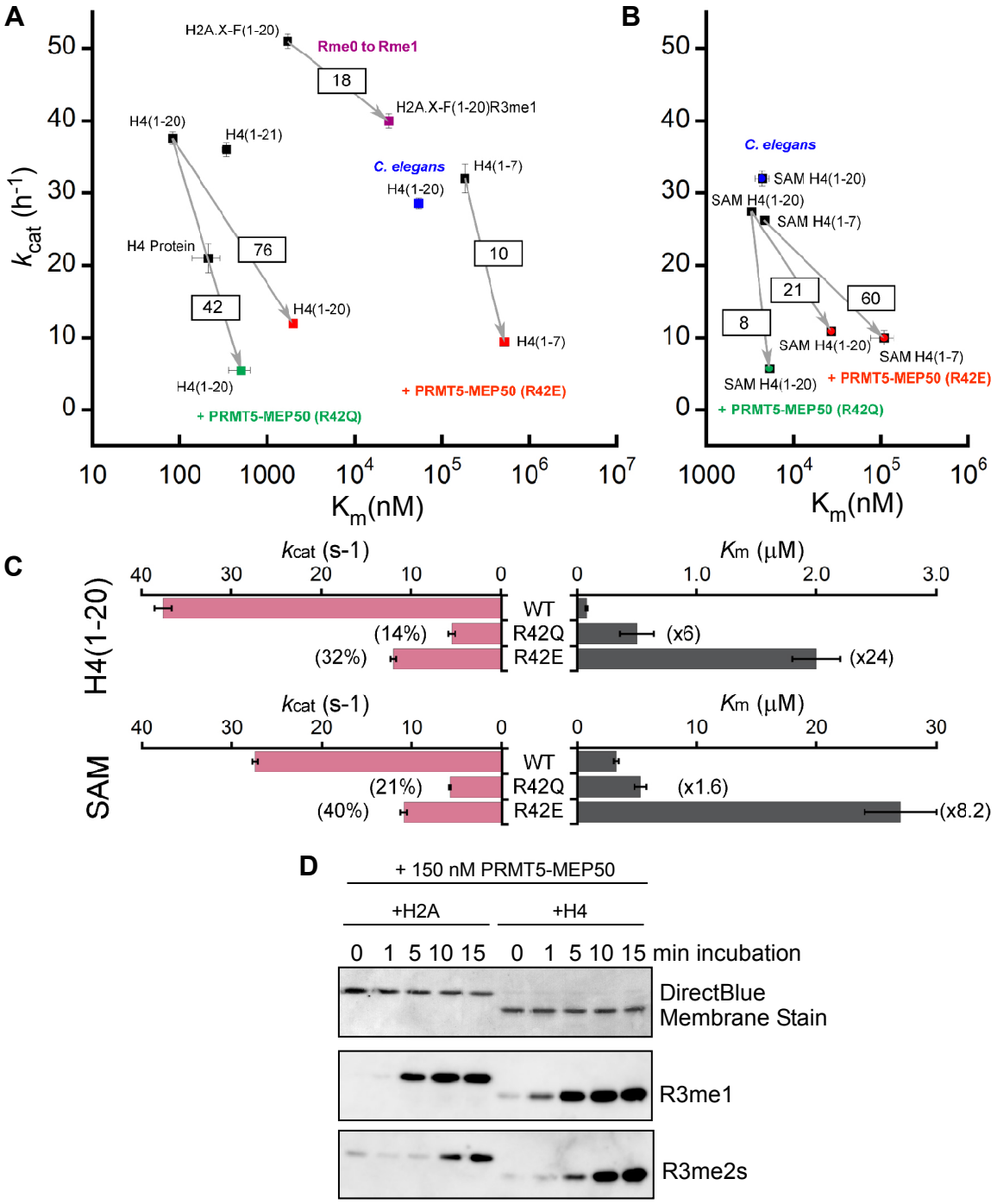

Figure 6

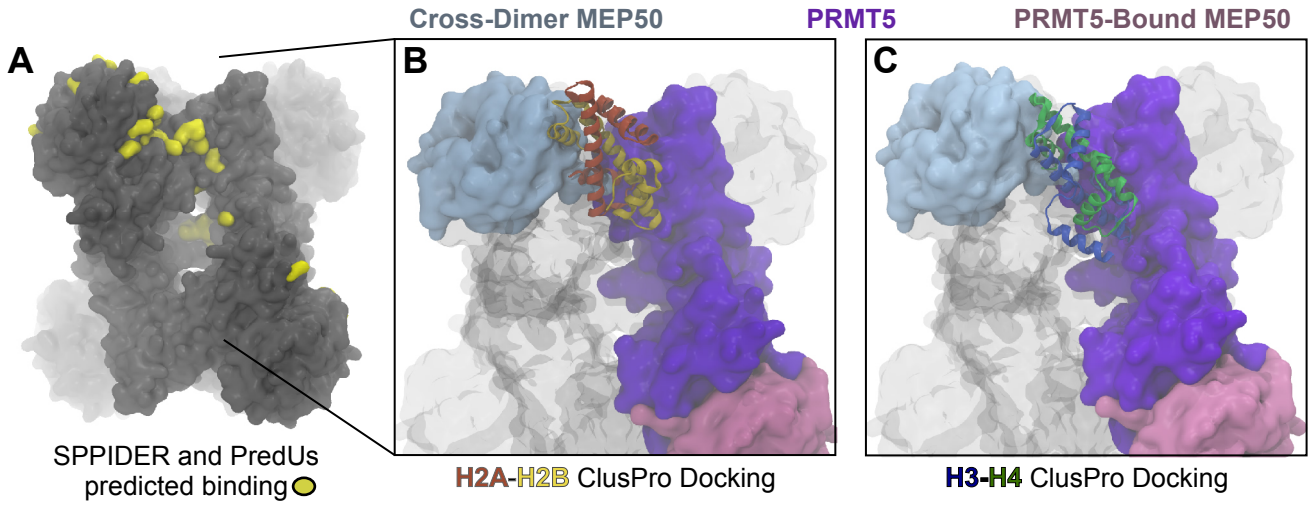

Figure 7

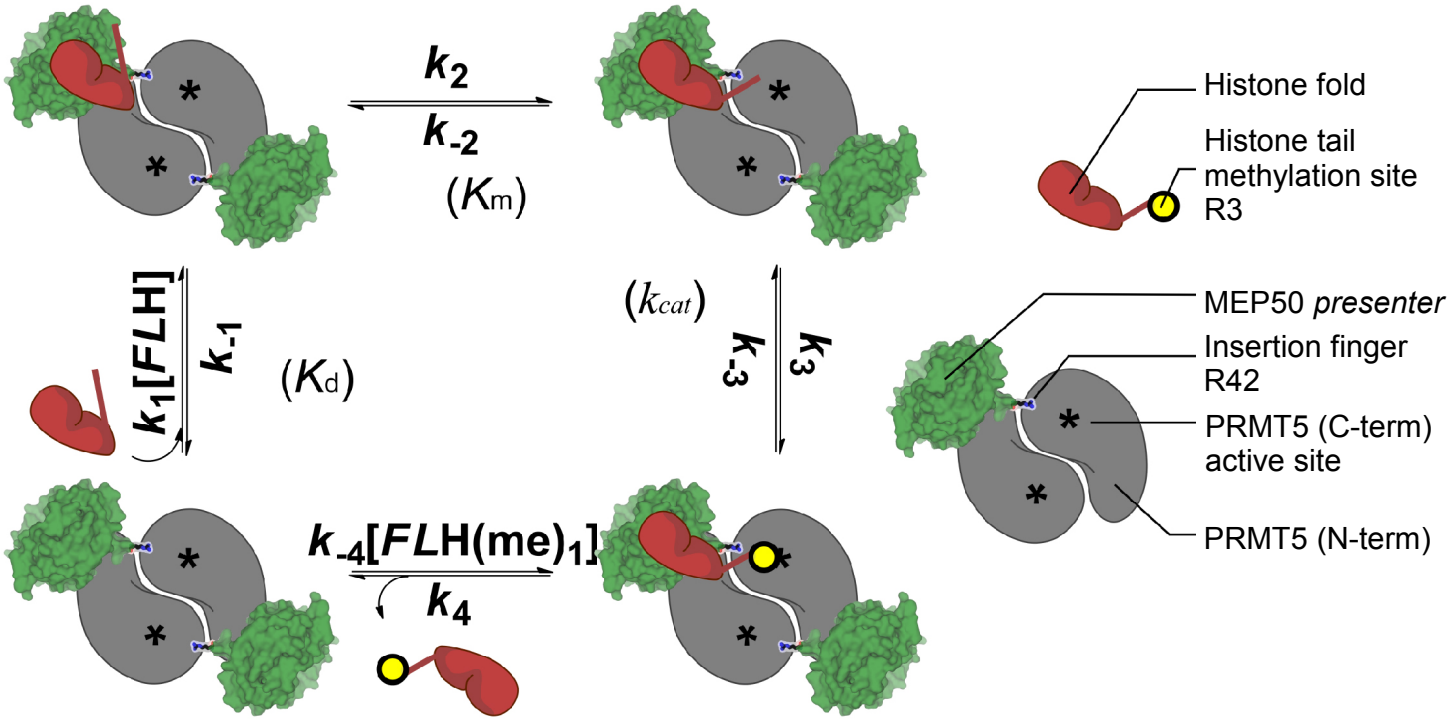

Figure 8

Enzymology:

Histone H2A and H4 N-Terminal Tails are Positioned by the MEP50 WD-Repeat Protein for Efficient Methylation by the PRMT5 Arginine Methyltransferase

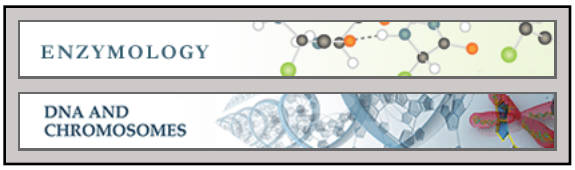

Emmanuel S. Burgos, Carola Wilczek, Takashi Onikubo, Jeffrey B. Bonanno, Janina Jansong, Ulf Reimer and David Shechter

J. Biol. Chem. published online February 24, 2015

Access the most updated version of this article at doi: 10.1074/jbc.M115.636894